ImpediBands: Body Coupled Bio-Impedance Patches for Physiological Sensing Proof of Concept

Kaan Sel, *Student Member, IEEE*, Bassem Ibrahim, *Student Member, IEEE,*
and Roozbeh Jafari, *Senior Member, IEEE*

***Abstract*— Continuous and robust monitoring of physiological signals is essential in improving the diagnosis and management of cardiovascular and respiratory diseases. The state-of-the-art systems for monitoring vital signs such as heart rate, heart rate variability, respiration rate, and other hemodynamic and respiratory parameters use often bulky and obtrusive systems or depend on wearables with limited sensing methods based on repetitive properties of the signals rather than the morphology. Moreover, multiple devices and modalities are typically needed for capturing various vital signs simultaneously. In this paper, we introduce ImpediBands: small-sized distributed smart bio-impedance (Bio-Z) patches, where the communication between the patches is established through the human body, eliminating the need for electrical wires that would create a common potential point between sensors. We use ImpediBands to collect instantaneous measurements from multiple locations over the chest at the same time. We propose a blind source separation (BSS) technique based on the second-order blind identification (SOBI) followed by signal reconstruction to extract heart and lung activities from the Bio-Z signals. Using the separated source signals, we demonstrate the performance of our system via providing strong confidence in the estimation of heart and respiration rates with low RMSE (HR_{RMSE} = 0.579 beats per minute, RR_{RMSE} = 0.285 breaths per minute) and high correlation coefficients (r_{HR} = 0.948, r_{RR} = 0.921).**

***Index Terms*—bio-impedance, chest, heart rate, physiological sensing, respiration, SOBI, source separation, wearable,**

I. Introduction

PREVENTION of many disorders requires sustainable and long-term health tracking [1]. In the case of cardiovascular and respiratory diseases, the symptoms of many complications are observed through the anomalies in the hemodynamic (*e.g.*, heart rate, heart rate variability, blood pressure) and respiratory parameters (*e.g.*, respiration rate, pulmonary volumes) [2]. Continuous and reliable monitoring of these biomarkers, such as heart rate (HR), blood pressure and respiration rate (RR) allows the early diagnosis and management or even prevention of the disease [3].

A significant challenge remains in building a continuous monitoring system that provides a convenient, non-obtrusive and non-invasive vital signs acquisition mechanism without restricting the mobility of the end-user for long-term operation. The current adopted bio-medical instrumentation is obtrusive and bulky, employing rather old technologies, requiring multiple sets of sensors and devices to provide a plurality set of vital measurements. This limitation directly impacts adherence to wearing the sensors over an extended period of time. Current wearables that focus on the convenience of wear implement modalities that can only capture skin surface observations [4]–[6]. These observations are not sufficient to capture certain hemodynamic and respiratory parameters with high-fidelity because activities of the small capillaries near the skin surface do not retain the information that major arteries would provide.

To address these gaps, we introduce ImpediBands: distributed smart small-size patches that can perform continuous measurements of global chest physiological signals for accurate estimation of hemodynamic and respiratory parameters with a single device. Our ImpediBand technology, as illustrated in Fig. 1, collects multiple instantaneous bio-impedance (Bio-Z) observations across different locations on the chest while establishing communications between the patches through the body. Therefore, the proposed method leverages the Bio-Z observations to determine a plurality of vital signs from the lungs and the heart. To measure Bio-Z, we apply a very small AC signal to the thorax and pick up differential voltages across multiple locations employing four-terminal sensing (Kelvin sensing). We chose Bio-Z sensing for non-invasive and high-fidelity physiological signal acquisition due to the higher penetration of the signals into the body as we will elaborate more in detail within Section II including the discussion on the limitations with the current state-of-the-art techniques. The variations in the Bio-Z signal corresponds to the periodic heart and lung activities, muscle contractions, and body fluid level changes, allowing to observe a holistic set of physiological measurements. Our specific work for ImpediBands offers a set of improvements over the traditional Bio-Z measurement systems, providing a more reliable and modular physiological data acquisition while enhancing the convenience and unobtrusiveness of the system for the end-users and support long-term wearability.

K. Sel and B. Ibrahim are with Department of Electrical and Computer Engineering at Texas A&M University, College Station, Texas, 77843, USA. ksel@tamu.edu, bassem@tamu.edu

R. Jafari is with Departments of Biomedical, Computer Science and Engineering, and Electrical and Computer Engineering at Texas A&M University, College Station, Texas, 77843, USA. rjafari@tamu.edu.

Our contribution in this paper can be summarized as follows:

- The ImpediBands are smaller-sized (3-inches) Bio-Z patches as compared to the convention (over 10 inches), while limiting the estimation error to less than a beat and breath-per-minute for heart and respiration rates (HR_{RMSE} = 0.579 beats per minute, RR_{RMSE} = 0.285 breaths per minute, r_{HR} = 0.948, r_{RR} = 0.921).
- The ImpediBands use a novel Bio-Z sensing technique over multiple locations through a single injection location to obtain a complete picture of physiological indicators.
- We use the set of multivariate observations acquired at different locations on the thorax to decompose the physiological sources based on their time coherence.
- Our proof of concept study demonstrates a wireless coupling between ImpediBand patches without the need for a shared reference or a common ground connection. Hence, the final design would eliminate the needs of chest-bands and/or wires connecting various bands, offering a convenient and comfortable form factor.

The rest of the paper is organized as follows. We present the previous related work and introduce the notion of Bio-Z in Section II. We share our methods and details of the experimental evaluation in Section III and Section IV respectively. We provide a discussion in Section V evaluating our performance and elaborating on the limitations and potential techniques to address the gaps. Finally, our conclusion is given in Section VI.

II. Related Work

Bioinstrumentation devices can be categorized into two different classes. The first class includes devices that are highly accurate and medical-grade yet bulky and immobile. The second class consists of wearable sensors and devices that provide unique opportunities for unobtrusive, low-cost and ambulatory sensing, but the challenge lies in the fidelity and robustness of the sensing and the fact that diverse physiological observations would require a plurality of sensors. Our proposed system directly addresses these gaps with improved accuracy and wearability (Section IV and Section V). In the remainder of this section, we discuss prior arts with respect to both classes of the physiological sensing paradigms. We then introduce an overview of the ImpediBands framework.

A. Current Practice for Physiological Monitoring

The current practices commonly used in clinics to measure hemodynamic parameters result in an inconvenience for the patient. Unfortunately, the current respiratory measurement systems rely on invasive and bulky sensors which are inconvenient for the patients. Nocturnal polysomnography (PSG) and capnography are two commonly used techniques for respiration monitoring, despite the obtrusive patient experience. PSG devices operate based on a technology that was developed in the 1960s, where respiration of the patient is monitored through sensor belts, measuring chest wall movements and upper abdominal wall movements through piezoelectric sensors

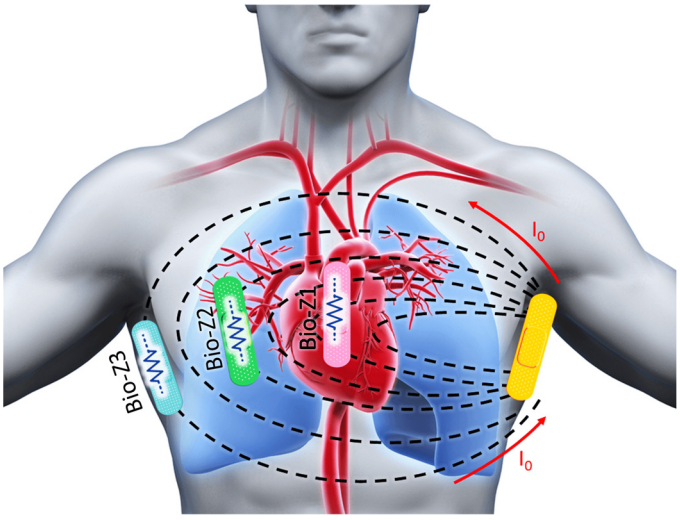

Fig. 1. ImpediBands: distributed Bio-Z sensors for continuous physiological sensing of hemodynamic and respiratory parameters to improve diagnostic and prognostic services. The ImpediBands establish the communication with each other through the human body using the known characteristics of the signal injection. [55]

[7], [8]. To acquire clean signals, these belts should be securely attached to the subject for the duration of the measurement, causing significant discomfort. In contrast, capnography systems measure RR by continuously monitoring CO_2 and O_2 gas exchanges with the help of nasal sensors or face masks, and however, the patient still undergoes an unpleasant experience [9]. In addition, these techniques are costly, requiring evaluation in specialized clinics. Moreover, both methods are *ad hoc* and require an extra set of sensors to measure additional vital signs such as heart activity and hemodynamic parameters.

Current wearable systems, in contrast to the previous practices, offer continuous and unobtrusive yet localized signal measurements from specific parts of the human body such as wrists, arms, and ankles to acquire heart rate (HR) and several other hemodynamic parameters [10]–[12]. The most widely used wearable systems rely on either electrocardiogram (ECG) or photoplethysmography (PPG) signals, for heart rate measurements. In the PPG based systems, the skin is illuminated with light at a certain wavelength and intensity; the intensity of the reflected/transmitted light is then measured at the receiver. The rate of the cardiac pump can be extracted from the variations in the received illumination magnitude. These variations are caused by the periodic changes of the blood volume mostly at the capillaries, as most of the time, the penetration of the light is not strong enough to reach the arterial sites [13], [14]. PPG can additionally provide insight into the respiratory parameters [16]–[20]. The respiration measurements from PPG sensors are due to the mixing of the PPG signal with the respiratory-induced variations of veins, caused by the alterations in intrathoracic pressure [21]. The main challenge in vital sign extraction, for example for RR, is the dependency of the target vital sign on the mixing quality, which is a factor of skin thickness, temperature, sensor locations, and many other parameters overall impacting the estimation accuracy. [22]. In addition, this mixing effect is usually very weak compared to the PPG signal amplitude,

decreasing the reliability and accuracy of the respiration signal extraction [23]. The electrical polarization, recorded with an ECG, can also provide the heart rate information with improved robustness to noise [25], [26], however same challenge remains when it comes to extracting ECG-derived respiratory activity inducing itself at the heart rate variability [4], [27], [28].

In addition to PPG and ECG, several investigations are focusing on modalities for noncontact measurement. These modalities still need to be close to the body. Examples include two groups of sensors to extract cardiorespiratory parameters; (a) respiratory-induced plethysmography (RIP) [29], [30], motion [31], acoustic [32], pressure/strain [33], [34], pyroelectric and triboelectric nanogenerator [35], [36], capacitive [37] and radio-frequency (RF) [38] based wearable systems and (b) those that are dependent on surrounding radar/Wi-Fi or Bluetooth stations [39]–[41]. The correct operation of the first group of sensors is dependent on their relative position to the body, their placement and environmental factors (humidity, temperature), and if ideal conditions are not created, they may suffer from low SNR. Station-based sensing systems that use radar and Wi-Fi signals additionally are not wearable and not suitable for scenarios where the user is moving due to the stationary requirements of their corresponding setups [25].

Bio-impedance is another non-invasive technique used in the physiological signal acquisition, where the method relies on an AC signal stimulation to the epidermis through electrodes and measuring a voltage difference across two points on the body. This allows the extraction of more information compared to optical modalities since it penetrates inside the body throughout its course. Therefore, it is possible to carry a holistic set of physiological measurements with Bio-Z, including but not limited to HR, heart rate variability (HRV), RR, muscle movements, and hydration level by capturing the variations induced by the muscle activities and concentration changes. Several studies in the literature measure vital signs related to blood flow such as heart rate, pulse transit time, and eventually, blood pressure [11], [12], [42], [43] using the current injection and voltage sensing electrodes lined up in one patch and located across the arm and wrist. Moreover, other studies estimate the respiration rate over a localized single patch [44]–[46]. However, extracting respiratory waves are somewhat challenging from these localized measurements since these systems can only measure variations of the impedance that are partially correlated to the respiratory cycle through arm and wrist motion and respiratory-induced blood flow, making the measurement sensitive to motion artifacts and placement of the electrodes. To obtain highly accurate measurements, it is essential to place the sensors on the actual sources of the respiration, which are the lungs. Electro-impedance tomography (EIT) or impedance cardiography (ICG) are methods that depend on placing two sets of injection electrodes on both sides of the neck and abdominals and two sensing electrode pairs across the upper chest to record the impedance changes over the whole chest area [47], [48]. The cardiac and ventilation readings, in this case, are stronger than the measurements taking place at different body locations, since the sensors directly sense heart and lung movements [49]. However, the major drawback of this system is the utilization of long wires all across the chest to establish an electrical connection between injection and sensing electrode pairs. Moreover, the patch sizes are more than tens of cm. Hence, the state-of-the-art sensing paradigms are not convenient for long-term monitoring, which is essential in providing more effective diagnostics and management of cardiovascular and respiratory diseases. A single patch can be placed on the chest to capture the respiration. However, such an approach captures a plurality of signal sources and with a single sensing site; various sources could not be separated effectively, especially when the frequencies of the physiological activities, as well as physical activities, overlap.

B. Overview of the ImpediBand Framework

ImpediBands leverage Bio-Z for non-invasive and high-resolution sensing to continuously estimate various vital signs including HR and RR. Unlike traditional Bio-Z systems that require an electrical connection between the injection and sensing electrode pairs, we eliminate all wired-communications between the patches to provide a convenient and comfortable experience to the users. Moreover, with the proposed method we are able to collect global measurements from the chest, where observations cover the upper body completely through the distributed patches without the necessity of utilizing any kind of chest band. We accomplish this by injecting the current signal from the side of the body and placing voltage sensing electrodes in parallel to the injection patch at different locations over the chest, rather than the uniaxial placement of sensing electrodes with respect to the injected signal. This kind of sensing configuration is proposed for the first time by our team to the best of our knowledge. Moreover, the novel placement of the ImpediBands over the chest provides multiple observation points and allows enhancement in the source estimation through blind source separation (BSS) techniques [50]. The term *blind* refers to the condition where only the information carried by the observations is known and used, with no information on the sources. Our ImpediBand Bio-Z patches placed over the chest capture an instantaneous mixture of the heart and lung activity sources. Hence, it is possible to separate Bio-Z signals generated by the heart and lungs to increase the fidelity and stability of the hemodynamic and respiratory parameter estimation, due to the strongly correlated information carried by the captured signals in time. To leverage this time coherence of the sources appearing in the observations, we apply a second-order blind identification (SOBI) algorithm using the second-order statistics of the observations and obtain both heart and respiration waves from the correlation analysis under a range of delay assumptions [51]. We then reconstruct the signals based on the estimated mixing matrix to extract both phase and frequency information of the sources. A detailed explanation of the iterative SOBI algorithm and the associated advantages are shared in the next section. Overall, ImpediBands provide a high-fidelity modular sensing mechanism while offering comfort and convenience to the end-user that justify continuous wear. In this paper, we demonstrate our device performance in

estimating HR and RR highly accurately, yet we do not specifically target characterizing the robustness of the system.

III. Methods

Through establishing electrical contact with the skin via electrodes, it is possible to stimulate the epidermis with an alternating electrical current. While this AC signal finds the least impeding path, at high frequencies it passes through a combination of extracellular fluid, cell membrane, and intracellular fluid, capturing a mixture of information about the physiological status [45]. This behavior can be modeled using an RC circuit as shown in Fig. 2, by representing the intracellular and extracellular fluids with resistors, R_I and R_E respectively, and the cell membrane as a capacitor, C_M in parallel to R_E and in series with R_I. Therefore, the frequency of the injected signal directly affects the impedance path, where at low frequencies the current will not be able to penetrate through the capacitive cell membrane, whereas at very high frequencies body will act as a low-pass filter [52]. Notice that, in the calculation of a transfer function from a cellular region, the ratio of RC parameters with respect to each other is more significant than the values themselves. There are several advantages of injecting a high-frequency AC signal into the epidermis. First, increasing frequency significantly decreases the electrode-to-skin impedance caused by the unideal current transfer between ions and electrons [53]. Therefore, the voltage drop across the electrodes at the injection side becomes minimal allowing higher amplitudes of current stimulation. Second, the allowance of injection amplitude before damaging the tissues increases with increasing frequency after 1 kHz (up to 100 kHz), as stated by the safety standards [54]. Third, changes in the impedance of the tissues and underlying cells due to physiological changes (blood flow, lung and heart movements, hydration, and muscle movements, *etc.*) will be carried by this higher frequency signal. In return, the flicker noise dominating the low-frequency spectrum will less distort the information carried by the injected signal. For all these aforementioned reasons, while still suffering from reasonable attenuation at the tissue impedance due to its low-pass behavior, we selected to work with 10 kHz for the Bio-Z measurements. We have verified this carrier frequency in our prior works [11], [55].

A. Simplified Impedance Modelling of the Thorax

A voltage pick-up sensor placed at the upper chest would reflect the variations in the Bio-Z signal based on the physiological autonomic motive forces (heart, lungs, pulsatile movement) as well as controlled muscle forces (respiration-based chest motion, stretching, *etc.*). Placing multiple of these sensors captures these activities from multiple locations with various contributions of each activity. This allows the application of advanced source separation techniques to separate these individual activities. To leverage the common information present in the multiple observations, we propose placing three Bio-Z sensors at different locations of the chest that pick-up the voltages induced by only a single current injection site located underneath the left armpit.

To be able to simulate our proposed approach, we created a simplified impedance mapping of the upper chest, where we only simulated the variations caused by the periodic activation

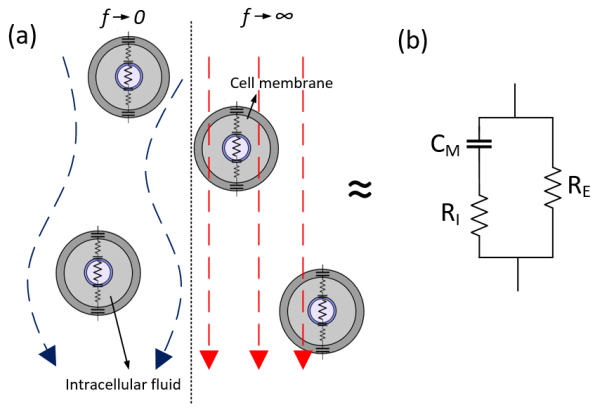

Fig. 2. Tissue impedance modelling (a) AC signal paths within the tissue intracellular (ICF) and extracellular (ECF) fluids, at low and high frequencies (b) Equivalent tissue impedance circuit.

of the heart and lungs at 1.3 Hz and 0.2 Hz respectively in the analysis, to match with our experimental data. In our simulations, the time constant of the tissue impedance is much smaller than the body impedance changes due to heart and lung activities ($\tau_{tissue} \approx \mu s \ll \tau_{heart/lungs} \approx s$). This is because the C_M, R_I and R_E values are on the order of nano-farads and tens of ohms, respectively for the tissue impedance block provided in Fig. 2 (b) [56]–[58]. Therefore, we were able to reduce the model complexity by replacing the tissue impedance block with a resistive element. With this simplification, the fastest frequency component is due to the time variant resistance (*i.e.* 1.3 Hz) instead of our original injection frequency of 10 kHz. Hence, the Nyquist sampling criterion requirement is relaxed by 5 orders of magnitude, allowing a larger time step selection for the simulation and significantly decreasing the number of samples per second.

The simplified impedance mapping consists of a resistive 10-by-13 matrix (130 elements in total) to represent the whole upper chest. Each element corresponds to two parallel resistive tissue blocks to include the possibility of representing regions with multiple organs (*i.e.* heart and lungs) associated with a single element. Each resistive tissue block is assigned to have a non-stationary part that is 5 orders of magnitude larger than the time-dependent part to match our experimental results as well as the previous work [55], [56]. Fig. 3 shows the model and the placement of the voltage pick-up sensors as well as the current injection point. Table I shows the values assigned for each resistive block.

We used LTSPICE to run the simulation and processed the differential voltage data in MATLAB. Fig. 4 shows the variations in the normalized sensor readings, where all sensors were able to capture the respiratory activity, no matter the sensor location. However, Sensor 3 shows a very weak response to the variations caused by heart activity both due to its location with respect to the heart and the injection point. We also shared the simulation results corresponding to the magnitudes of lung and heart activities appearing within the differential voltages picked-up over different columns in Fig. 5. For this simulation, we only changed the columns of the sensors, whereas the rows of the differential points of the voltage sensors remained unchanged at rows 4 and 9 as in Fig. 4. The simulation results show that the peaks for heart activity and lung activity do not necessarily need to happen at the same sensing point, justifying

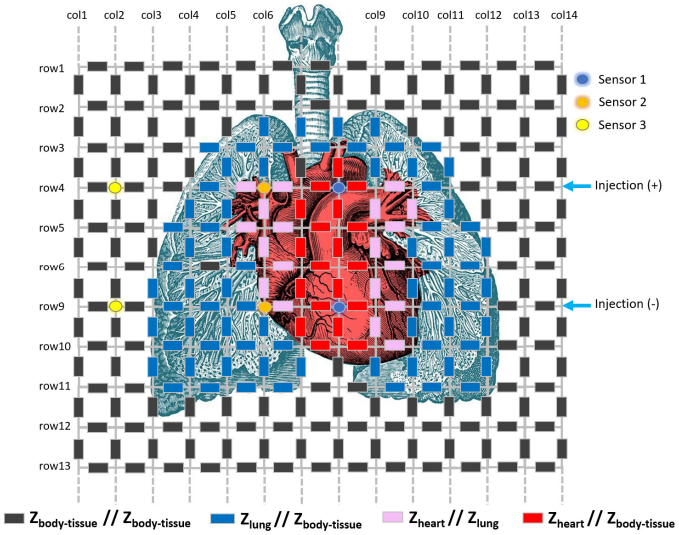

Fig. 3. SPICE based impedance modelling of the upper chest. Each element represents a resistive value. Depending on the location of the element, resistance becomes time varying.

TABLE I
VALUES ASSIGNED FOR DIFFERENT RESISTIVE ELEMENTS

Element annotation	Assigned resistance value ($m\Omega$)
$Z_{body\text{-}tissue}$	10^4
Z_{heart}	$Z_{body\text{-}tissue} + 25\sin(2\pi \cdot 1.3 \cdot time)$
Z_{lung}	$Z_{body\text{-}tissue} + 50\sin(2\pi \cdot 0.2 \cdot time)$

placing multiple patches across different locations, which we employ in the ImpediBands framework. Hence, our approach allows capturing a holistic set of observations directly from the sources. In addition, it allows creating a diverse mixing matrix, where although the exact locations of the sources are unknown, leveraging through our iterative-SOBI algorithm it is possible to estimate these source activities. Moreover, this analysis shows that although the exact values of the voltage electrode placement, as well as the current flowing through each element, may also remain unknown, the impedance variations are still appearing at the differential voltage nodes. The fundamental purpose of the simplified chest modeling shared here is to demonstrate the components (physiological sources) that appear in the Bio-Z sensing across different locations. However, the model is not dedicated to providing an accurate representation of the amplitudes of each component in the observations. In addition, this simulation is a simplified 2D model and the exact location of the peaks may change in the real case and from subject to another based on the chest anatomy. Since it is challenging to determine the exact location of the peak in advance, we needed to consider the placement of the sensors at arbitrary locations on the chest.

B. Multi-Channel Bio-Impedance Sensing

The Bio-Z sensing of the ImpediBands consists of two parts, which we refer to in this paper as the transmitter (TX) and the receiver (RX). The TX is responsible for the generation of a programmable AC current for injection into the human body, with controlled gain and amplitude. As the current passes through the chest, it induces a voltage sensed by the RX patches located at different locations over the chest. Separating the

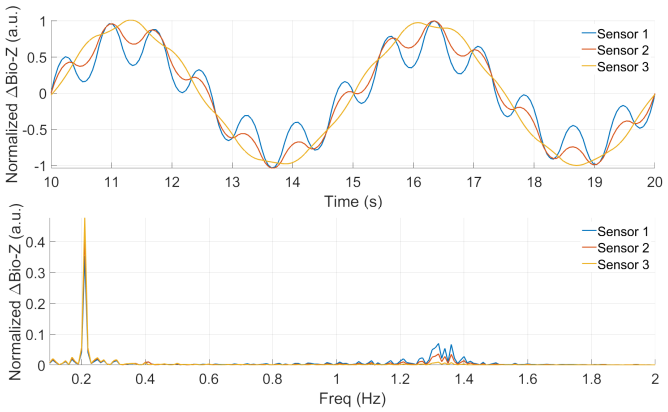

Fig. 4. LTSPICE simulation results that show the variations in the sensor voltages based on their location on the upper body. All sensors reflect the simulated activities of the heart and lungs at 1.3 and 0.15 Hz, respectively.

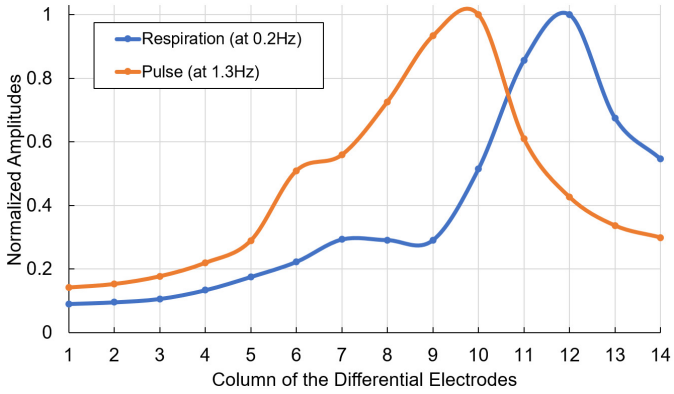

Fig. 5. LTSPICE simulation results for voltage pick-up sensors placed at different columns of row 4 and row 9.

injection and sensing electrodes leverage the four-point sensing mechanism to mitigate the effect of the electrode-skin interface, which is commonly used in previous related work [46], [48]. This is because the sensing electrodes usually followed by a buffer or instrumentational amplifier (IA) with a very high input gain rejecting a current flow to its input. Therefore, the voltage drop across the sensing patches caused by a portion of the injected current that is passing through the underlying Bio-Z will be buffered to the output with negligible loss and interference.

The current injection and the voltage sensing are established using small-sized (24 mm diameter) pre-gelled (wet) circular Ag/AgCl electrodes. To ensure that the ImpediBand patches remain comfortable to wear, we separate and electrically isolate the TX and RX patches from each other, by giving up the phase calibration between the injection site and the sensing sites. Since our injection and sensing patches do not contain a common potential, only the frequency information is known by the sensing patches. This is enough to carry out a phase insensitive lock-in based amplitude demodulation to fully capture the variations in the Bio-Z signal. These variations correspond to the physiological signals initiated by the periodic heart and lung movements, which are the focus of this work. Consequently, the phase calibration becomes insignificant. To provide a reference point to the differential inputs of the RX, we also connected the circuit ground of the RX patches to the

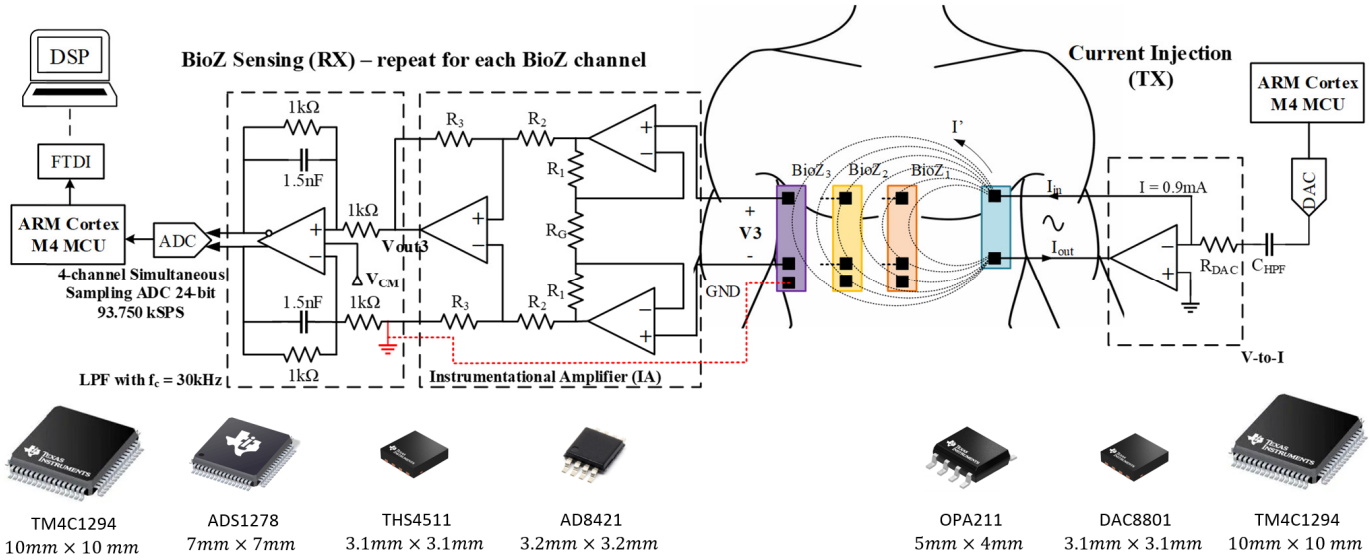

Fig. 6. Multi-channel low noise Bio-Z sensing hardware. Both current injection and voltage sensing patches depend on the ARM Cortex M4 MCU. The patches do not share any electrical connection between each other and the earth ground. In order to improve the signal quality, we use extra electrodes to connect circuit GND with the body. [55] The choices of components support a small factor custom-developed PCB with a wearable form factor. The design can easily be integrated into a custom-developed PCB to get a wearable form factor.

body using our electrodes. This improves the common-mode rejection ratio, by preventing the amplification of the floating common-mode signals and increasing the received SNR at the RX (Section IV).

The TX and RX hardware are shown in Fig. 6, where both depend on discrete components for the proof of concept. Both patches incorporate an ARM Cortex M4 MCU and operate through a small size battery and a power management board designed in our lab. The TX MCU is responsible for running a 16-bit DAC (DAC8811, Texas Instruments, USA) to generate an AC signal (with programmable frequency) with its output amplitude based on a reference generator set at 5.1 Volts giving 80 μV resolution. The DAC operates at low power with $I_{DD} =$ 2 μA. A capacitor is placed at the output of the DAC to prevent DC injection into the skin. This voltage signal is then converted to the electrical current through a 5.1 kΩ resistor fed to the negative input of a low power precision amplifier (OPA211, Texas Instruments, USA) of 1.1 $nV/\sqrt{Hz}$ noise density at 10 kHz with 45 MHz gain-bandwidth product ($G = 1$) with positive input being grounded. The amplifier supports low power applications with a typical supply current of 3.6 mA. The injection bio-potential electrodes are connected to the feedback loop of the op-amp, allowing 0.7 mA rms current flow at the digital normalized gain of one, which can be set through PC. To comply with the safety standards at 10 kHz, we used 0.64 mA rms as our injection amplitude [54].

The amplitude of the variations in the Bio-Z signal due to blood flow is very small at approximately 50 $m\Omega$ with several inches of electrode separation. Therefore, we designed the RX of our ImpediBand system with low-noise Bio-Z sensing hardware using discrete components. Each RX patch includes two sensing electrodes to measure the accumulated voltage difference due to the current flow induced by the injected AC signal. This voltage is then amplified with a low noise (3.2 $nV/\sqrt{Hz}$ input voltage noise at 10 kHz) and low power (2.3 mA maximum supply current) instrumentational amplifier (AD8421, Analog Devices, USA) at the gain set to 20 dB with 110 dB common-mode rejection ratio (2 MHz bandwidth). It is then provided to an ADC after passing through a low-pass anti-aliasing filter with cut-off frequency at 30 kHz. For improved data acquisition, we selected a high-resolution and high-speed delta-sigma ADC (ADS1278, Texas Instruments, USA) that samples three independent Bio-Z channels simultaneously at 93.75 kSPS with 24-bit resolution (0.3 μV sensing resolution, with 9 points per signal period). The ADC can operate in low power mode with a power dissipation of 31 mW/ch. In this work, we use a single multi-channel ADC to carry out all analog to digital conversion, which does not violate the idea of wireless communication between the patches, due to the isolated processing of each individual analog channel. A single RX patch with the current HW configuration consumes less than 0.3 A at 5 V during active mode and can support 3 hours of continuous operation with no duty cycling with ultra-low power step-up converter of above 90% efficiency (MAX8627, Maxim Integrated, USA) and 3.7V 1000mAh thin LiPo battery (LP256258, LiPol Battery Co., China). The battery life can be further expanded with the duty cycling of sensing. As the fundamental purpose of this paper is to demonstrate a proof of concept, we did not further investigate the power optimization. Nevertheless, we discussed our plans for optimal power-management for the final form factor of the ImpediBands in Section V. The acquired signals are then transferred to a PC through USB communication (FT223H, Future Technology Devices International Ltd, USA) for digital signal processing (DSP) and extracting heart and respiration activities. We first tested the system with a 4.4 $k\Omega$ resistor (representing both of the electrode-to-skin impedances, [53]) in series with 50 Ω resistor as the load, where we connected the two ends of the 50 Ω resistor to the IA to extract the noise characteristics and to find the Volts to Ohms gain of each of the channels. Our noise

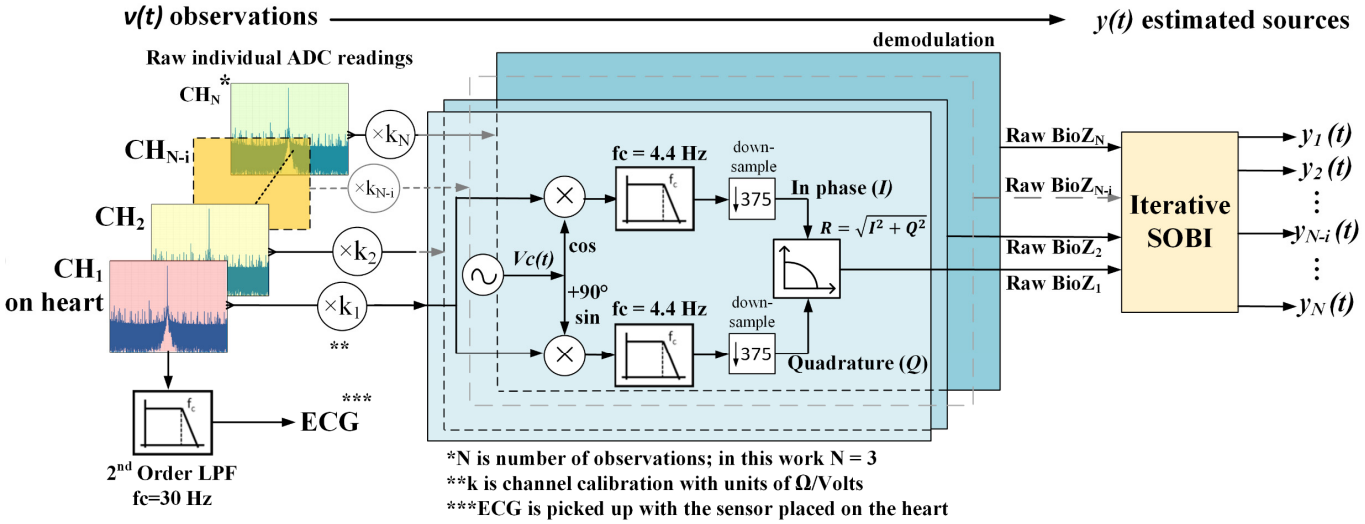

Fig. 7. Block diagram of our signal processing stages carried in MATLAB.

measurements across this known calibration resistor show that the system is capable of acquiring Bio-Z measurements with a root mean square (RMS) error less than 1 $m\Omega$, which is sufficiently lower than the target Bio-Z variations (50 $m\Omega$).

All DSP operations are carried out in MATLAB for our proof of concept prototype, where a corresponding flowchart is shown in Fig. 7. The proposed DSP operations can be ported and executed on local MCUs. Since the phase information is lost due to the electrical isolation between RX and TX patches, we carry a lock-in based demodulation, followed by a second-order Butterworth low-pass filter with 4.4 Hz cut-off to reject the image noise, as well as high-frequency fluctuations, while accepting the heart rates up to 180 beats per minute (bpm). We then down-sample the signals from 93.750 kHz to 375 Hz. After the demodulation, we obtain three simultaneous Bio-Z measurements at different locations and distances to the heart and lungs. The details of the patch placement and patch sizes are shared in the Results section of this manuscript. This allows us to apply blind source separation (BSS) techniques to separate the signals sourced independently by heart and lungs from each other using the multiple simultaneous observations. In this paper, we introduce a variation of SOBI leveraging the information on the second-order statistics of the Bio-Z observations and the prior knowledge on human physiology to separate and extract heart and respiration rates. The reason we selected SOBI is due to its success in using the time coherence of the source signals appearing in the observations with different time delays. Moreover, SOBI is robust to the time delay variations of the sources for each observation. These unknown delays are introduced due to blood flow being present at various parts of the chest but with different phases and the capacitive components of the Bio-Z sensing.

In addition to low-noise and high-fidelity Bio-Z sensing, our system takes advantage of the sensor placement on the chest to capture ECG signals without any extra effort. ECG is a biopotential signal appearing at the baseband of the measured voltages with our Bio-Z sensors located at the chest. To obtain the ECG signal, we apply a second-order Butterworth low-pass filter with a 30 Hz cut-off frequency. We use ECG as a reference for our HR measurements. However, it is also possible to calculate systolic time intervals with the timing information on ECG and Bio-Z signals using a localized measurement at the heart. This requires studying the morphology of the periodic heart activity signals and is planned for the future.

C. Iterative Source Separation using Second Order Blind Identification (SOBI)

Our proposed physiological sensing approach brings out a holistic set of observations that are linear projections of both physiological and physical sources. In the literature, to extract the underlying sources in these linear mixtures, which resemble vital signs or other signals of interest, several BSS techniques are developed. Independent Component Analysis (ICA) is a commonly used technique for feature extraction [59], audio signal processing [60], and also blind source separation for noise rejection in EEG and EMG signals [61]–[63]. Moreover, in our prior work, we utilized ICA for separation of heart and lung sources modulating the Bio-Z based observations, with the assumption that the sources are statistically independent [55]. This is usually not the case for physiological sources. In addition, ICA, due to its statistical behavior, is highly sensitive to the difference in phase delays appearing on the observations associated with the blood flow and introduced through capacitive components of the Bio-Z sensing. Several studies in the literature attempt to combat the phase delay by introducing latency-insensitive versions of ICA, however at a trade-off of loss of information or accuracy [64]–[66].

Bio-Z measurements over a large chest area demonstrate high variances in terms of phase delays since blood arrives at different time instances to each sensing location, which limits the utility of ICA and other purely statistical methods. Second-order separation (SOS) techniques contrast with this feature of statistical methods, where the separation takes place due to the temporal characteristics in the ongoing activity of the underlying sources [67]. In order to enhance the robustness of the SOS algorithms and combat the ambiguity in the time delays introduced by the human body, an effective method is to

run the algorithm multiple times, with a set of preselected time lags introduced to the signals before each run. SOBI is a promising SOS technique exploiting the temporal coherence of the underlying sources with different spectral contents to perform their separation from each other [51]. Since it is based on joint diagonalization of multiple covariance matrices with different time delays, instead of a single unique matrix preferred in other SOS techniques, it significantly improves the robustness in determining the heart and lung sources at low processing cost [51], [68]. We leveraged this feature of the SOBI in our study to get better estimates of the sources.

The input data can be represented as a vector of N recorded signals, $v = [v_1, v_2, \dots, v_N]^T$, as the observations of M unknown independent sources, $s = [s_1, s_2, \dots, s_M]^T$. This instantaneous linear mixture can be modeled through an $n \times m$ mixing matrix, $\mathbf{A}$ as,

$$v(t) = \mathbf{A} \times s(t) + n(t) \quad (1)$$

Here, $n(t)$ represents the additive noise modeled under two assumptions: (i) source signals $s(t)$ and noise $n(t)$ are statistically independent, (ii) $n(t)$ is white, stationary and with zero mean [69]. Second-order statistics-based source separation techniques leverage the temporal correlations between the observations. Hence they provide an advantage for scenarios where the observed signals retain low SNR, mainly because the noise is not common between these observations and does not significantly impact the correlation estimations [51]. In addition, noise elements that are not Gaussian can be added to the source estimation problem.

SOBI only uses this array of observations, without any prior knowledge of the model, to find the mixing matrix to get the estimated and uncorrelated sources, $y = \hat{s}$. In order to obtain $\mathbf{A}$, SOBI starts with the whitening process of the observations to reduce the determination of the $n \times m$ mixing matrix $\mathbf{A}$ to a unitary $m \times m$ matrix, $\mathbf{U}$, without any loss of generality, using the whitening matrix, $\boldsymbol{W}$ [51].

$$\mathbf{A} = \mathbf{W^T} \times \mathbf{U} \quad (2)$$

Then, within a preset time delay window, τ, the algorithm calculates a set of covariance matrices. We selected the τ to be 100, corresponding to a ±13 ms time window, with our sampling frequency of 375 Hz after the down-sampling. This step is followed by a joint diagonalization analysis to find the orthonormal change of basis [69]. At the output, the matrix with the highest sum-squared cross-correlation value is selected as the first estimated component, and the iteration continues until all m components are determined. Bio-Z measurements across the chest provide a strong reflection of the respiration [55]. This reflection is captured from all of our sensors simultaneously. In addition, each sensor captures a set of other internal and external sources such as heart movements, blood flow, motion artifacts and other biopotential signals, which do not necessarily appear with the same temporal structure in the observations. Due to the strong appearance of the respiration cycle in the temporal characteristics of the Bio-Z signals, the very first estimated source at the output of the SOBI that has the highest eigenvector gives the respiratory signal. In addition to the sources, SOBI estimates the mixing matrix, which allows us to isolate the appearance of each source in the observations. We perform reconstruction of the Bio-Z observations by removing the contribution of the respiratory activity extracted by SOBI for each observation using the demixing matrix that is the inverse of mixing matrix. The resulting signals include the temporal information of the heart activity without any disturbance on the phase characteristics (*i.e.* delayed arrival of heart pressure pulse wave at different locations of the thorax due to finite pulse wave velocity). The iterative SOBI algorithm that includes the reconstruction is presented in Algorithm 1.

Algorithm 1 Iterative Second Order Blind Identification (SOBI) for phase and frequency recovery of the physiological sources.

Input: raw Bio-Z signals $v(t) = [BioZ1(t), BioZ2(t), Bioz3(t)]$ that are observations of the system

Output: estimated sources $y(t)$, *mixing matrix* $\mathbf{A}$

1. $z(t) = \mathbf{W} \times v(t)$ // whitening
2. ***for j = 1 to τ do:*** // adding time delays to observations, τ = 100
3. $R_z[j] = E\{z(:, j:N) \cdot z(:, 1:N-j)^H\}$ // estimate correlation matrix for the given time lag
4. **end for**
5. $\hat{\mathrm{U}} \leftarrow$ joint diagonalization of $\{R_z[k_j] \mid j = 1, \dots, \tau\}$ with the minimum sum-squared off diagonals
6. $\mathbf{A} = \mathbf{W}^{\mathrm{H}} \times \hat{\mathrm{U}}$ // estimating mixing matrix
7. $y(t) = \mathbf{A} \times v(t)$ // estimating sources
8. $BioZR(t) = y_1(t)$ // first estimated source corresponding to the respiratory activity
9. $\mathbf{I} = \mathbf{D} \times \mathbf{A}$ & $v(t) = \mathbf{D} \times y(t)$ // get demixing matrix that is the inverse of estimated mixing matrix
10. $BioZH(t) = v_1(t) - \mathbf{D_{nx1}} \times y(t)$ // subtract the contribution of the respiratory part from the Bio-Z signal to obtain heart activity with its unique phase

D. Peak Detection, HR and RR Estimation

We use the reconstructed Bio-Z based heart activity signal to estimate the HR. First, we extract the spectrogram of each signal using FFT and detect a dominant frequency region. We then apply a second-order Butterworth low-pass filter with a cut-off frequency that is 1 Hz higher than the dominant frequency to reject the high-frequency oscillations. To calculate the HR, we use the zero-crossing, foot and peak points of the first and second derivatives of the signal to detect the important characteristic points, such as local peaks, feet and maximum slope points (MSPs). We use these points to calculate the corresponding interbeat intervals (IBI). IBI is effectively the period or the duration of one heartbeat. We apply a similar peak detection algorithm to the ECG signals to measure the reference IBIs. In order to reduce the effect of motion artifacts, we apply a moving average filter to the inverse of the calculated IBIs (1/IBI, beats per second) with a 30-second averaging window and 28 seconds of overlap to both Bio-Z and ECG signals. We multiply the output of each window by 60 to obtain the HR value in beats per minute (bpm) for each 30-second window.

For the respiration signal detected by the SOBI algorithm, we apply an additional second-order Butterworth low-pass filter at 1 Hz, to remove the high-frequency oscillations, followed by a peak detection algorithm to calculate inter-breath intervals

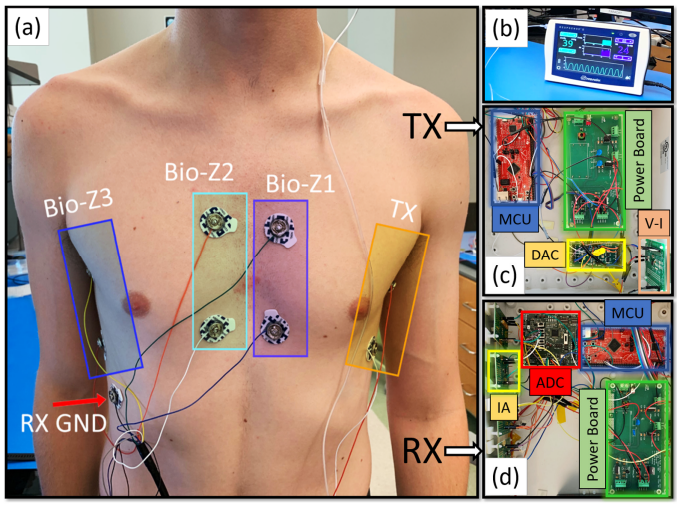

Fig. 8. (a) Placement of the ImpediBand TX and RX patches for data collection from multiple locations over the chest. (b) In addition, we used capnography utilizing a nose cannula to measure CO_2 changes and gold standard respiration. (c)-(d) ImpediBands TX and RX prototypes for proof of concept study.

(IBrI) similar to IBIs. In order to provide an average estimate of the RR for a preset interval, we apply a 60-second averaging window to the calculated IBrIs with 55 seconds of overlap.

IV. Experimental Results

In order to evaluate the performance of the system, we used ImpediBands to extract continuous HR and RR values from 10 healthy human subjects under the IRB approval IRB2017-0086D by Texas A&M University. Prior to the main experimental study, we first evaluated the performance improvement with the body GND electrode placement and conducted two pilot studies to decide on the optimum patch size and to show the importance of multiple patch approach rather than single patch measurements. The patch size is critical in understanding the limitations of our system and to demonstrate the feasibility of suitable electrode size/separation for enhanced wearability. A smaller electrode separation on a single patch leads to a direct decrease in the size of the patch supporting the wearable applications built on top of this technology with a trade-off in the SNR. In addition, the multiple patch approach proposed in this paper is essential in providing high-fidelity separation of heart and lung activities.

We provide a detailed explanation of the data collection protocol utilized in our experiments, the source separation performance of our system as well as the results of each aforementioned study in this section.

A. Data Collection

As discussed in the earlier sections, we implemented a novel sensing technique with the ImpediBand patches to provide global observations of the chest physiology. We achieve this through two main steps. First, the injection electrodes within the TX patch were placed underneath the left armpit. Second, with the assumption that all parts of the upper body see a fraction of this current, we place three RX ImpediBand patches at different locations of the upper body as shown in Fig. 8. The first RX patch (Bio-Z1) was placed across the heart (left of the sternum), the second patch (Bio-Z2) was placed at the right of

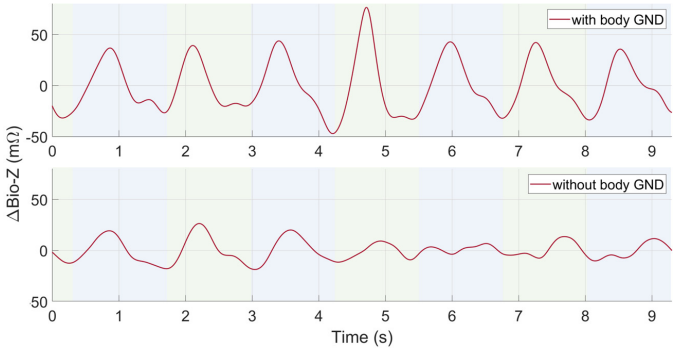

Fig. 9. Flipped ΔBio-Z signals with and without GND electrode placed at the body. The placement of body GND electrode improves the signal fidelity.

the sternum and the last Bio-Z sensor (Bio-Z3) was placed underneath the right armpit, giving full coverage across the chest. The electrode placement was performed by the subjects themselves over the dedicated areas to ensure their own comfort level. Such a case also demonstrates the realistic variations in the placement for each individual. In all our Bio-Z measurements, we inject a sinusoidal at 10 kHz with 0.64 mA rms amplitude, complying with the safety standards [54].

To evaluate the effect of GND electrode placement of the RX patches on the body, we run two one-minute long experiments with the only difference between the experiments being the inclusion of the GND electrode. For both experiments, we used the TX patch for the injection and Bio-Z1 for sensing. Since the voltage pick-up is differential, the location of the GND electrode is not significant. On the other hand, the GND electrode is placed next to the RX patch to prevent the patch size increase. Under the same injection amplitudes, we observed that the SNR of the carrier signal, picked-up by the TX patch with the body GND electrode is 7 dB higher than the case without the body GND electrode since GND electrode improves the common-mode rejection of the IA [70], [71]. Fig. 9 shows the flipped ΔBio-Z signal after the demodulation for both cases. The signal fidelity is better with the body GND electrode, in agreement to the SNR measurements. Consequently, moving forward we used the body GND electrodes placed next to the RX patches with no constraint on the precise placement.

For the pilot study regarding the size of the ImpediBand patches, we tested the effect of the separation amount between differential electrodes (nodes) of each patch from 1-inch to 5-inches under a total of 25 minutes of data collection from a single subject. Moving forward, we used 3-inches separation between the two differential nodes of each TX and RX patches, due to its superior performance compared to the smaller sizes while providing similar performance compared to the larger sizes. The results of this study are shared in the following subsections. In order to complete an extensive evaluation of the ImpediBands, we collected four sets of five-minute continuous data from 10 healthy subjects.

To assess the performance of ImpediBands for estimating the HR, we used the ECG signal captured simultaneously by the Bio-Z1 sensor placed at the heart to detect the true heartbeats. Moreover, we used capnography (RespSense II, Nonin, USA)

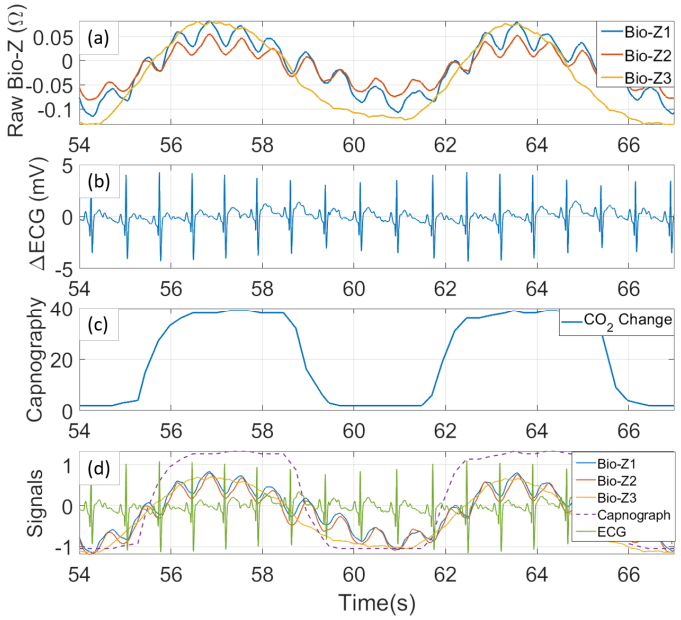

Fig. 10. (a)-(b) Time plots of the measured physiological signals with ImpediBand and (c) the reference capnography measurement. All Bio-Z sensors are reading an instantaneous mixing of the underlying sources (heart and lungs signals). (d) All signals scaled and plotted within the same time legend.

for measuring a reference of the respiration waves recorded during the data collection with ImpediBands to assess our estimation of RR. The capnography tracks the CO_2 concentration through a nasal cannula connected to the device to determine the RR. During the whole data collection process, subjects remained seated with the capnography device connected through a nasal cannula. Prior to the start of the actual data collection with the ImpediBands, we asked subjects to hold their breath for 10 seconds, where we used this signature time interval to synchronize capnography data to the ImpediBands data.

B. Source Separation

An example of the physiological signals measured with our setup and the capnography device is shown in Fig. 10. We clearly observe periodic lung movements due to respiration on the raw Bio-Z signals captured by the ImpediBand patches. Therefore, we expect iterative SOBI to identify this significant temporal correlation between the sensors with high fidelity. Fig. 11 shows an exemplary frequency spectrogram correlating the raw Bio-Z inputs that are sent to iterative SOBI, the respiration and heart activity signals obtained through iterative SOBI. We also plot the corresponding references for both sources in the figure. After the application of the iterative SOBI algorithm with the signal reconstruction, the system estimates heart and lung activities with high accuracy. The separated heart (Bio-ZH) and respiration (Bio-ZR) source signals ($y(t)$) were used in HR and RR estimations, respectively.

C. Peak Detection, Inter-Beat and Inter-Breath Interval Estimation

An example of the extracted characteristics points on the Bio-ZH and Bio-ZR signals, and on the corresponding reference signals are shown in Fig. 12. We calculate IBIs from a

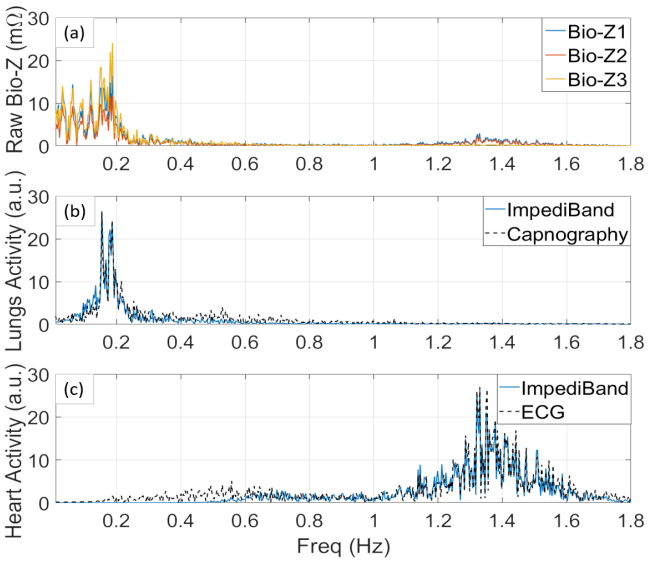

Fig. 11. The frequency spectroscopy of the input and output SOBI signals. (a) The raw Bio-Z signals are modulated by the respiration cycle with the additional frequency components appearing at higher frequencies. (b) It is observed that, the respiration signal obtained after the application of source separation is matching with the reference signal acquired through capnography. (c) Moreover, the heart activity signal estimated after signal reconstruction exhibits an improved SNR matching with the reference ECG signal.

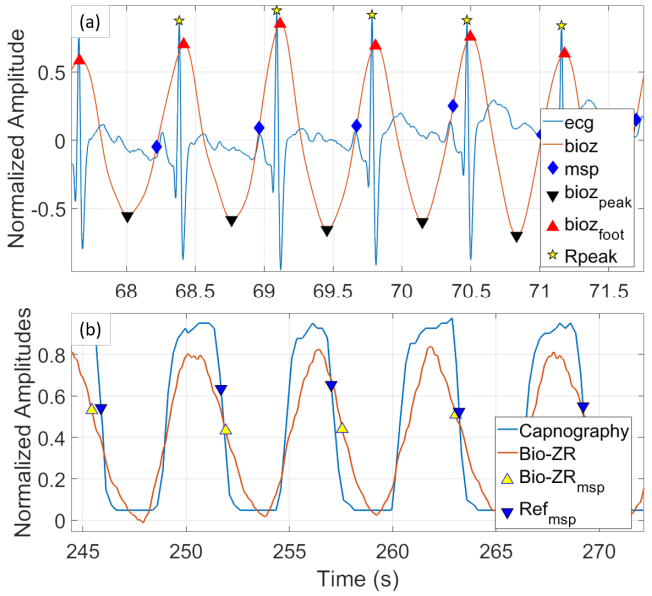

Fig. 12. (a) Feature extraction from Bio-ZH with reference ECG and (b) Bio-ZR with reference capnography signals. An example of the extracted points from the physiological signals are shown with different colors in the plots.

combination of maximum slope point (MSP), peak and footpoints in Bio-ZH and R-peaks in the ECG signal. To estimate IBrIs from the Bio-ZR and capnography signals, we use the MSPs. In order to mitigate the effect of motion artifacts and high-frequency oscillations that alter the peak points, we apply the moving average algorithm presented in Section III.C.

D. Effect of Patch Sizes in Device Performance

1) Respiration Rate

The Pearson's correlation coefficient (r) and average root mean square error (RMSE) in breaths-per-minute (BPM) in RR

TABLE II
SIZE-PERFORMANCE COMPARISON IN RR AND IBRI ESTIMATION

Patch Size (inches)	RR		IBrI		
	r	RMSE (BPM)	Upper 95% limit (s)	Lower 95% limit (s)	r
5	0.961	0.167	0.444	-0.389	0.961
4	0.914	0.112	0.439	-0.464	0.914
3	0.912	0.067	0.274	-0.283	0.912
2	0.904	0.299	0.785	-0.605	0.904
1	0.962	0.183	0.549	-0.482	0.962

TABLE III
SIZE-PERFORMANCE COMPARISON IN HR AND IBI ESTIMATION

Patch Size (inches)	HR		IBI		
	r	RMSE (bpm)	Upper 95% limit (ms)	Lower 95% limit (ms)	r
5	0.976	0.267	6.16	-6.95	0.976
4	0.980	0.325	9.15	-4.87	0.984
3	0.983	0.655	17.1	-18.9	0.983
2	0.751	3.697	124.3	-25.6	0.765
1	-0.122	5.217	189.2	-67.2	-0.090

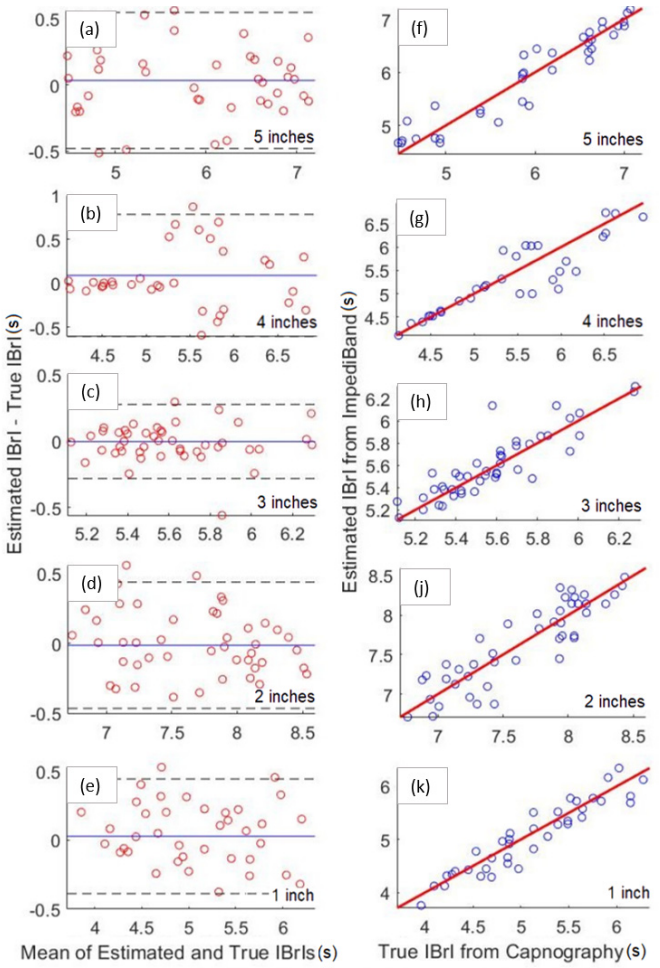

Fig. 13. (a)-(e) Bland-Altman and (f)-(k) Pearson's correlation analyses plots for different patch sizes to evaluate the RR estimation performance. IBrI refers to inter-breath interval. From (a) to (e) and (f) to (k) the patch sizes are selected as 5-inches, 4-inches, 3-inches, 2-inches and 1-inch, respectively for both analyses.

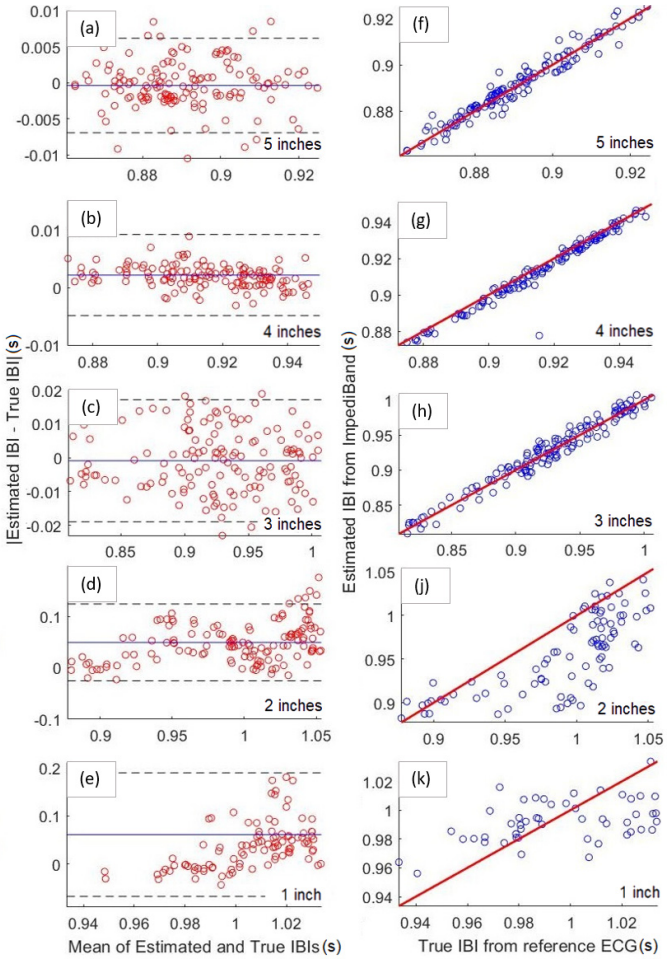

Fig. 14. (a)-(e) Bland-Altman and (f)-(k) Pearson's correlation analyses plots for different patch sizes to evaluate the HR estimation performance. From (a) to (e) and (f) to (k) the patch sizes are selected as 5-inches, 4-inches, 3-inches, 2-inches and 1-inch, respectively for both analyses.

estimation for five different patch sizes that are determined by the separation between the differential electrodes of each patch starting from 5-inches up to 1-inch are provided in Table II. The Bland-Altman and Pearson's correlation analyses for this pilot study are given in Fig. 13. For each plot, we used 51 IBrIs calculated from the averaged peak-to-peak values. We observe that ImpediBands provide strong confidence in RR estimation with all patch sizes with a minimum of 0.9 correlation and a maximum of 0.3 BPM RMSE.

2) Heart Rate

We share the *r* and RMSE in bpm in HR estimation for all patch sizes starting in Table III. Results show that the device performance with higher than 3-inches patch separation remains comparable with an RMSE of less than one bpm. However, in contrast to RR estimation performance, further decreasing the size from 3-inches to 2-inches degrades the signal quality and increases the error in HR estimation. Fig. 14 shows the corresponding Bland-Altman and Pearson's correlation plots for different patch sizes using 140 IBIs for each size. The 95% limits of agreement are also given in Table III. We used 3-inches patch size to move forward with the extensive analysis due to the high accuracy in both HR and RR estimations using this configuration.

E. Performance Evaluation of ImpediBands over Multiple Test Subject

1) Respiration Rate

We used 1377 IBrIs in the analysis, where we excluded data for subjects 7 and 9 in the analysis due to peak detection problems and very high noise in the dataset for these subjects, respectively. Moving forward, we present *r*, RMSE in BPM and average BPM for each subject in Table IV. In Fig. 15, we provide the plots for Bland-Altman and Pearson's correlation analysis over 1377 IBrIs. The results show a strong agreement between our method and the reference method, where the negative and positive 95% limits of agreement values appeared less than 1.3 BPM, with the mean of the error ($IBI_{estimated} - IBI_{true}$) appearing as 0.07 BPM. In addition, Pearson's correlation analysis resulted in 0.983 for the correlation coefficient, *r*.

2) Heart Rate

In the performance evaluations, we used 3798 IBIs calculated using more than 2 hours of data collection in total from seven healthy subjects. For this evaluation, we excluded data corresponding to Subjects 1 and 9 due to high divergence from the rest of the subjects. In addition, we observed an anomaly in ECG of Subject 5, also detected with the ImpediBand sensors. For this reason, we separated Subject 5's data from the dataset. To indicate the agreement between the ECG and Bio-ZH acquired with the ImpediBands, we compared the averaged IBIs for both signals. Table V provides the average RMSE in bpm and *r* for each subject in HR estimation. The results demonstrate a strong correlation of estimated HR with the reference HR for each subject, with average *r* appearing at 0.948 and RMSE at 0.579 bpm. In order to conduct a comprehensive analysis of the IBI estimation performance, we carried the Bland-Altman and Pearson's correlation analyses over 3798 IBIs. We share the Bland-Altman plot in Fig. 16, showing a strong agreement between our technology and the gold standard. The 95% limits of the agreement appear at 22.1 ms and -22.4 ms. Pearson's correlation plot is also provided in the same figure with Pearson's correlation coefficient of 0.998.

F. Effect of the Number of Patches in Heart Activity Estimation Accuracies

In order to evaluate the performance improvement with our method with respect to the traditional methods that depend on a single patch measurement, we run a pilot study on a single subject over 20 minutes of data collection. With the subjects at rest, we placed the sensors as showed in Fig. 8 and carried the lock-in based demodulation separately for each sensor to extract the raw Bio-Z signals. We then define three different methods to extract the heart activity. The first method runs a 2nd order Butterworth filtering with a cut-off at 0.5 Hz on a single patch Bio-Z, whereas second and third methods depend on the application of iterative SOBI on two patches and three patches (proposed method) respectively. To evaluate the performance in separating the heart activity, we performed precision and recall analysis on estimated peak locations from the output signal and the true peak locations extracted from the ECG, as well as the Bland-Altman and Pearson's correlation analyses on the estimated IBIs and the true IBIs. For the filtering case with a single patch, we chose the patch placed on the heart to get the strongest heart activity, and for two patches based iterative

TABLE IV
RR ESTIMATION PERFORMANCE FOR EACH SUBJECT USING IMPEDIBANDS

Subject	r	RMSE (BPM)
1	0.978	0.097
2	0.893	0.294
3	0.919	0.292
4	0.892	0.364
5	0.935	0.128
6	0.962	0.559
8	0.848	0.365
10	0.944	0.181
Average	0.921±0.042	0.285±0.151

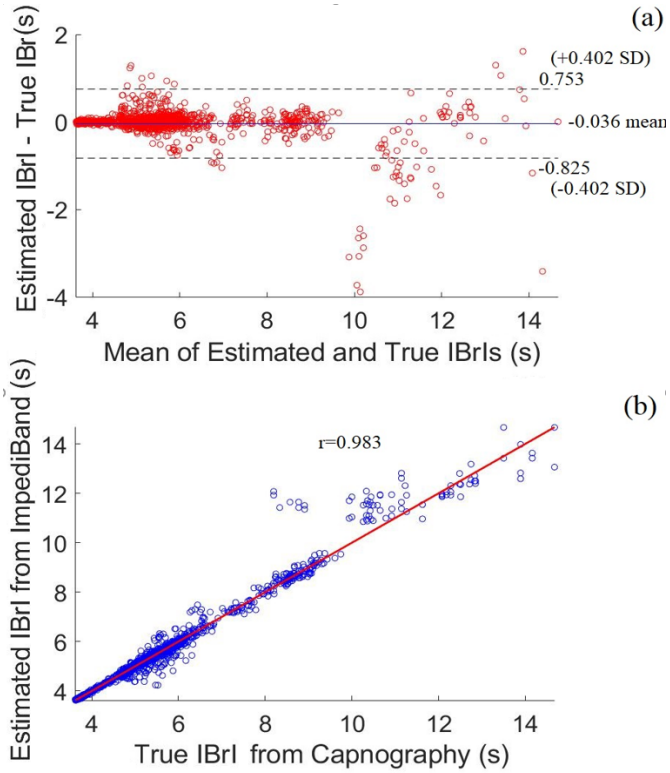

Fig. 15. IBrI estimation performance evaluation with ImpediBands in reference to capnography. (a) Bland-Altman plot is shared. The positive and negative 95% agreement points appeared at 0.753 s and -0.825 s respectively. (b) Pearson's correlation plot is shared, showing a very strong correlation of IBIs estimated from ImpediBands with the reference capnography measurement (r=0.983).

TABLE V
HR ESTIMATION PERFORMANCE FOR EACH SUBJECT USING IMPEDIBANDS

Subject	r	RMSE (bpm)
2	0.982	0.503
3	0.999	0.068
4	0.955	0.572
6	0.913	0.751
7	0.851	1.260
8	0.942	0.644
10	0.997	0.257
Average	0.948±0.053	0.579±0.380

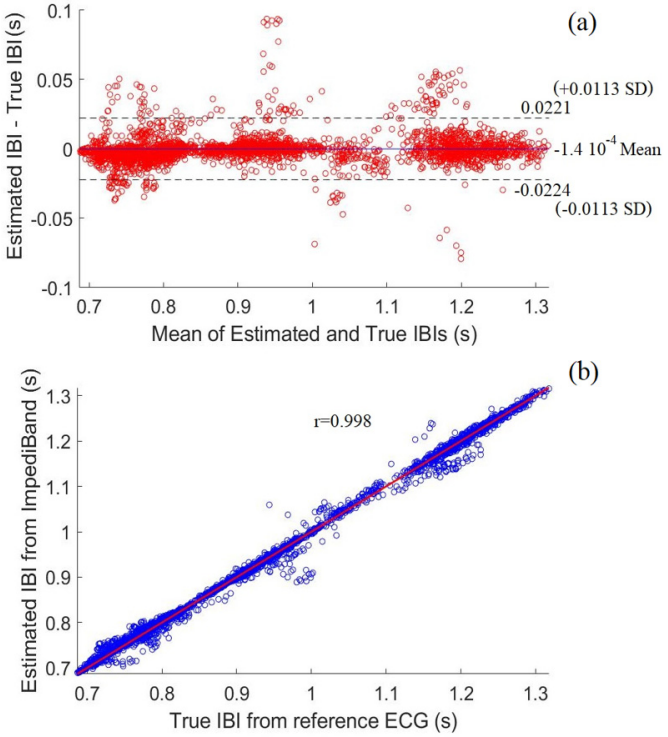

Fig. 16. IBI estimation performance evaluation with ImpediBands in reference to ECG. (a) Bland-Altman plot is shared. The positive and negative 95% agreement points appeared at 22.1 ms and -22.4 ms respectively. (b) Pearson's correlation plot is shared, showing a very strong correlation of IBIs estimated from ImpediBands with the reference ECG (r=0.998).

SOBI, we tried all three input combinations and took the average.

1) Precision and Recall Analysis on Peak Detection

We used 1988 beats in the analysis, where we applied our peak detection algorithm to the output signal for each method and the reference ECG signal. Based on the time location of each of the estimated peak with respect to the reference peak, we classified them as true positive (TP), false positive (FP) or false negative (FN). The TP, FP, and FN refer to the cases where the estimation falls in between 20% of the current beat in reference to ECG peak, falls outside of this 20% threshold and no peak is found inside this threshold, respectively. We then calculated the accuracy and precision as,

$$\text{Accuracy} = \frac{\text{TP}}{\text{TP} + \text{FP}} \tag{3}$$

$$\text{Precision} = \frac{\text{TP}}{\text{TP} + \text{FN}} \tag{4}$$

After this classification, we also calculated the RMSE based on the TPs only, where the error is defined as the difference between the IBIs calculated through reference versus estimated peaks. Fig. 17 shows the accuracy, precision, and RMSE obtained for each method, where the proposed method performs the best in all analysis metrics. In addition, SOBI even with two patches shows a significant improvement compared to the traditional filtering approach.

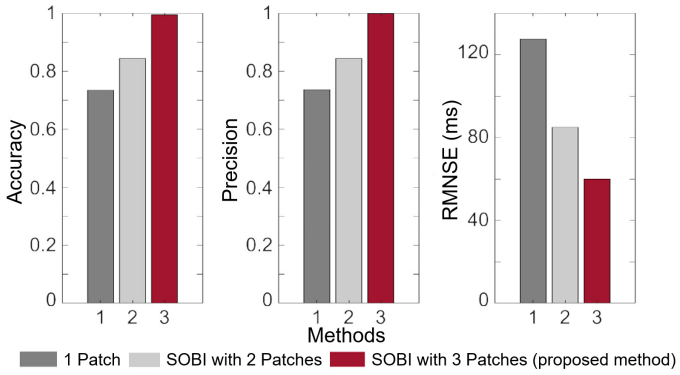

Fig. 17. Precision and recall analysis for the traditional method vs. proposed method, where the average IBI is 931 ms. 1 Patch experiment uses the Bio-Z1 patch placed on the heart to get the strongest heart activity. SOBI with 2 patches setting is the average of the all three input combinations (i.e. Bio-Z1 & Bio-Z2, Bio-Z1 & Bio-Z3, Bio-Z2 & Bio-Z3).

TABLE VI
PATCH NUMBER DEPENDENT PERFORMANCE COMPARISON IN IBI ESTIMATION

Method	IBI				
	Lower 95% limit (ms)	Mean Error (ms)	Upper 95% limit (ms)	r	RMSE (%)
1 Patch with 2^{nd} order Butterworth HPF	-107.12	3.95	115.03	0.8658	6.1%
2 Patches with iterative SOBI	-108.85	1.14	111.13	0.8780	6.0%
3 Patches with iterative SOBI (proposed method)	**-81.87**	1.68	**85.24**	**0.9184**	**4.5%**

2) Bland-Altman and Pearson's Correlation Analyses on Beat-to-Beat IBI Estimation.

In this analysis, instead of classifying estimated peaks with respect to the reference peak, for each reference peak, we chose the closest estimated peak, followed by beat-by-beat IBI calculation for both reference and estimated signals. We used 1295 IBIs in the analysis. Moving forward, we present *r*, RMSE and Bland-Altman coefficients in Table VI. In Fig. 18, we provide the plots for Bland-Altman and Pearson's correlation analysis over all IBIs. The results show a significant improvement in the agreement between our method and the reference method compared to filtering.

V. DISCUSSION AND FUTURE WORK

Overall our results demonstrate that the ImpediBands perform HR and RR estimations high accurately with an average RMSE of 0.288 BPM and 0.589 bpm for HR and RR, respectively. We also demonstrated the performance of the system under various electrode separation configurations and patch sizes. Our pilot study indicated that the 3-inches patch separation is sufficient for high fidelity signal acquisition. Moreover, it is still possible to use 1-inch patches to extract the respiration rate. The bio-impedance modality used in this paper is explored in the context of this application for the first time by our team. Other modalities were investigated by other research groups to extract respiration activity. These groups looked into

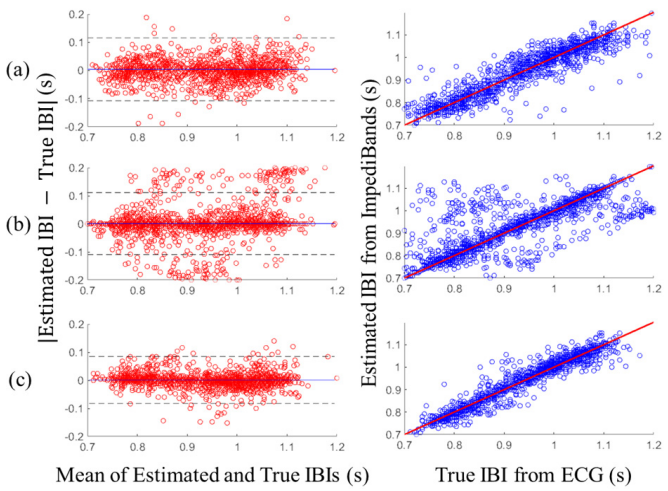

Fig. 18. Bland-Altman (right) and Pearson's correlation (left) plots for different number of patches. (a) 1 patch with 2^{nd} order Butterworth HPF with 0.5 Hz cut-off frequency. (b) 2 Patches with iterative SOBI. (c) 3 Patches with iterative SOBI (proposed method).

the frequency content to extract the average BPM respiration rate. In contrast, this work analyzes the individual breaths to extract the IBrI relations. Nevertheless, we compared our RR estimation accuracy with the state-of-the-art works as shared in Table VII.

This work presents a proof of concept rather than the realization of a final device. Therefore, we leveraged discrete components in order to facilitate fast prototyping and retain the flexibility of adjusting circuit parameters to maximize the performance of the system. The choices of components, however, as described in the paper, support a small factor custom-developed PCB with a wearable form factor. In this work, we carried out the data processing in MATLAB, with the data transferred through USB communication. The data processing requires point-wise multiplications for demodulation purposes, multiple second-order IIR filtering, and application of iterative-SOBI. Iterative-SOBI algorithm requires τ+3 iterations of X by N and N by X matrix multiplication for a single source estimation, with τ, X and N being the time delay window, number of observations and number of samples, bringing up a computational complexity that is linear with the number of samples (*i.e.*, $O(\tau X^2 N)$). We believe most modern MCUs can handle this computational complexity. Processing the data points on chip can also eliminate the USB communication with an external processing unit, a required step for the final wearable form factor. In order to achieve real-time operation with the proposed method, we offer running the iterative-SOBI algorithm over a sliding window with a latency less than 100ms (for real-time experience) that is almost an order of magnitude larger than our time-delay window (13 ms). Our system updates the HR and RR values every two and five seconds, respectively due to the usage of sliding window averaging. Two improvements can be performed in the future: (1) implementing a better peak detection algorithm to eliminate sliding window averaging in heart and respiration activity signals, (2) increasing the SNR by injecting/sensing from all patches at the same time, which will multiply the number of observations. These improvements will be tested by our team in future studies. In our setup, we employed a single ADC to carry out all analog to digital conversion. This does not violate the idea of wireless communication between the patches since the ADC inputs are differential voltage signals fed by a buffer isolating each individual channel. In this work, we did not focus on the power optimization of the ImpediBand patches. However, we chose low-power analog components while building the patches. In addition, the power consumption of the digital components can be improved further through various duty-cycling techniques [72], [73]. Moreover, carrying out the demodulation of the RX signals in analog settings (*e.g.* AD630, Analog Devices, USA) will reduce the sampling rate and will decrease the power consumption of the digital modules. The final version of the ImpediBand system requires building a fully wearable prototype with optimized power consumption and an extensive study on the types of electrode selection, such as e-Tattoos that provide intimate and seamless contact with the skin [53].

There are several novelties introduced with ImpediBand technology. First, the ImpediBands TX and RX patches do not carry a common potential and completely isolated from each other, for the first time in the literature. This improves the wearability of the system significantly and eliminates the dependency on chest bands to carry the wiring between patches. On the other hand, it results in a loss of the phase part of the body tissue impedance. However, two points can be argued here. First, the cardiorespiratory activities are relative and repetitive changes that also appear as relative changes in the measured Bio-Z, therefore time synchronization of TX and RX is not significant for such activities. Second, for applications where body phase response becomes important (*i.e.* dehydration and body muscle/fat mass measurements), an additional signal at higher frequencies (*i.e.* higher than 1 MHz) can be modulated with the actual injection signal at the desired frequency for time synchronization at the beginning of the measurements. In addition, we introduce a novel sensing technique to gather more information from the chest, where we used a single injection underneath the left armpit and measured the Bio-Z variations from multiple locations that are parallel to the injection patch. Compared to the traditional methods where all the injection and sensing remain within a local region with electrodes placed over a single line, this parallel configuration of the patches allowed us to collect multiple instantaneous observations of the underlying sources from different angles and distances. On the other hand, since the injection and sensing patches are physically separated from each other by a significant distance, the injected current suffers from dissipation over the other parts of the body. Nevertheless, with a low-noise sensing system, we show that even a small portion of the injected signal is sufficient to extract the hemodynamic and respiratory activities. Moreover, the appearance of the sources in the sensing sites is shown by the initial 2-layer SPICE simulation. The simulation results are in agreement with the experimental output of our system. We are working on a more precise chest modeling with more added layers and higher unit-resolution. In our previous work, we showed promising results for 3-D electrical modeling of the wrist in [56], which we plan to extend the study to the chest in the future.

In this paper, we introduce an iterative application of the SOBI, to leverage multiple simultaneous observations and the strong appearance of the respiratory muscular movement,

TABLE VII
RR ESTIMATION ACCURACY COMPARED WITH THE STATE-OF-THE-ART METHODS

Method	Sensor location	RMSE (BPM)	r	ME ± SD (BPM)
ECG (Welch spectrum) [27]	Abdomen	-	-	0.90 ± 1.26
PPG (Fourier spectrum) [23]	Forehead	-	-	1.80 ± 1.10
PPG (Holo-Hilbert spectrum) [19]	Wrist	-	-	0.04 ± 0.96
Radio-frequency (near-field coherent) [38]	Xiphoid process	3.45	-	-
Capacitive pressure sensor [37]	Face mask	2.26	-	-
ICG (empirical mode decomposition) [49]	Upper body	-	0.729	-
Bio-Z (ICA) [55]	Chest	-	-	0.97 ± 1.21
This work (Bio-Z, iterative-SOBI)	**Chest**	**0.29**	**0.921**	**0.04 ± 0.40**

improving our previously reported blind source separation performance as well as the convention. In our previous work, we used ICA for the separation of these sources and obtained an RMSE of 1.48 bpm for HR and 0.97 BPM for RR estimation [55]. ICA is a statistical method, which is highly sensitive to the latency variations within the observations due to the presence of finite blood flow velocity and capacitive part of the Bio-Z signal. In this work, we improved the existing signal processing by implementing iterative SOBI instead of ICA, which exploits the temporal coherence of the observations under multiple time delays to obtain the uncorrelated sources. In addition, considering temporal dependency rather than statistical dependency provides a better estimation of the sources of the measurements, under unideal mixing conditions where observations are dominated by a single source (i.e. respiratory activity due to lung movements). Our iterative SOBI algorithm improves the convention that depends on a straightforward application of SOBI to estimate all of the sources including the heart activity, which would be an averaged signal due to temporal mismatch of the source at different sensor locations. Instead, we reconstruct the observations by suppressing the respiratory contribution. Therefore, our method allows recovering both frequency and phase information of the heart activity and blood movement, in comparison to the previous techniques that were only able to extract the periodicity of the signals due to this inevitable averaging. Hence, we can further use the Bio-Z signals to extract hemodynamic features like pulse transit time (PTT), pulse wave velocity (PWV), aortic valve opening (AO), left-ventricular ejection time (LVET), and other parameters that depend on temporal characteristics of the signals. We compared our method that utilizes three Bio-Z patches with a single Bio-Z patch. The results show a significant improvement in the estimation performances with our method. In addition, we show that placing three patches is higher fidelity than placing two patches although followed by the same signal processing flow. This is expected as the inclusion of an extra sensor that provides an additional observation point will result in better source separation. For extreme cases, where signals suffer from high disturbance caused by other physiological changes, as well as motion artifacts, the number of ImpediBand patches can be increased to provide additional fidelity to the estimation performance.

The state-of-the-art technique in measuring chest impedance, the impedance cardiography (ICG), uses electrodes placed over the neck and the side abdomen to carry a global measurement of various including all of the underlying chest sources. In this study, we also focus on the chest vital signs with our smaller-size injection and sensing patches. In the future, we will compare our approach with ICG in acquiring modalities other than HR and RR (*e.g.* systolic time intervals, cardiac output). In our work, we also electrically isolated the injection patches from the sensing patches, for the first time.

One limitation of this study is that all our data collection was performed on healthy subjects. An extensive performance evaluation over a variety of test subjects is essential. Our system leverages from Kelvin sensing technique to isolate the Bio-Z measurements from the contact impedance variations. Hence the system performance becomes insensitive to the interface changes between the skin and the Ag/AgCl electrodes, due to changing temperature, humidity, and other external factors. However, human activity might still be picked up by the Bio-Z sensors due to tissue impedance changes with the muscle activations. Placing the sensors across different locations of the chest will expose sensors to the motion artifacts at different levels and temporal characteristics. Hence, the iterative-SOBI algorithm becomes less sensitive to these artifacts, while searching for the temporal correlations between the observations. In order to avoid the detonation caused by the motion artifacts, our testing protocol requires subjects to stay still while taking measurements. This might look like a limitation of the work, however, our objective in this paper was not the motion artifact rejection. A more comprehensive investigation with the inclusion of motion should be conducted in the future to obtain a better understanding of the system performance under extreme conditions. On the other hand, the literature has shown the importance of nocturnal physiological sensing [74]. In addition, the respiration studies are preferably performed during sleep to prevent bias introduced by the subject [75]. Therefore, it is reasonable to assume that the interference of the motion artifacts will be less critical at nighttime.

VI. CONCLUSION

ImpediBands provide global measurements across the chest with superior accuracy in terms of capturing the periodic heart and lung movements. Moreover, this measurement technique enables new research questions concerning Bio-Z signal morphologies and physiological modeling and their prognostic and diagnostic values. We evaluated the performance of our system on 10 healthy subjects over 3 hours of data collection. We compared the HR and RR estimation accuracy with the ECG recorded with the ImpediBands and capnography,

respectively. The results showed a strong correlation and small RMSE of r=0.998 and 0.58 bpm in HR estimation and r=0.983 and 0.20 BPM in RR estimation compared to the gold standards. We demonstrated that ImpediBands provide reliable and continuous physiological sensing ability while offering a convenient experience to the users in terms of wearability. ImpediBands accommodate long-term monitoring to improve the diagnosis and management of cardiovascular and respiratory diseases. In the future, we will perform further analysis to determine the hemodynamic parameters (i.e. cardiac output) and systolic time intervals (pre-ejection period, left ventricular ejection time, dZ/dt analysis). These measurements will create new opportunities and use-cases for the adoption of our technology to improve the quality of care.

ACKNOWLEDGMENT

The authors would like to acknowledge Alexander Brown for his help in the data collection.

REFERENCES

[1] T. Reichlin *et al.*, "Early diagnosis of myocardial infarction with sensitive cardiac troponin assays," *N. Engl. J. Med.*, vol. 361, no. 9, pp. 858–867, 2009.

[2] K. M. Anderson, P. M. Odell, P. W. F. Wilson, and W. B. Kannel, "Cardiovascular disease risk profiles," *Am. Heart J.*, vol. 121, no. 1, pp. 293–298, 1991.

[3] C. C. Burt and J. E. Arrowsmith, "Respiratory failure," *Surg.*, vol. 27, no. 11, pp. 475–479, 2009.

[4] P. H. Charlton, T. Bonnici, and L. Tarassenko, "An assessment of algorithms to estimate respiratory rate from the electrocardiogram and An assessment of algorithms to estimate respiratory rate from the electrocardiogram and photoplethysmogram," *Physiol. Meas.*, vol. 37, no. 610, 2016.

[5] M. A. Sackner *et al.*, "Calibration of respiratory inductive plethysmograph during natural breathing," *J. Appl. Physiol.*, vol. 66, no. 1, pp. 410–420, 1989.

[6] A. V. Moço, S. Stuijk, and G. de Haan, "Skin inhomogeneity as a source of error in remote PPG-imaging," *Biomed. Opt. Express*, vol. 7, no. 11, p. 4718, Nov. 2016.

[7] R. Nelson, "Scientific Basis for Polygraph Testing," *Polygraph*, vol. 44, no. 1, pp. 28–61, 2015.

[8] V. Ibáñez, J. Silva, and O. Cauli, "A survey on sleep assessment methods," *PeerJ*, vol. 6, p. e4849, 2018.

[9] R. Ortega, C. Connor, S. Kim, R. Djang, and K. Patel, "Monitoring Ventilation with Capnography," *N. Engl. J. Med.*, vol. 367, no. 19, p. e27, Nov. 2012.

[10] S. S. Thomas, V. Nathan, C. Zong, K. Soundarapandian, X. Shi, and R. Jafari, "BioWatch: A noninvasive wrist-based blood pressure monitor that incorporates training techniques for posture and subject variability," *IEEE J. Biomed. Heal. informatics*, vol. 20, no. 5, pp. 1291–1300, 2016.

[11] B. Ibrahim and R. Jafari, "Continuous Blood Pressure Monitoring using Wrist-worn Bio-impedance Sensors with Wet Electrodes," in *2018 IEEE Biomedical Circuits and Systems Conference (BioCAS)*, 2018, pp. 1–4.

[12] B. Ibrahim, A. Akbari, and R. Jafari, "A novel method for pulse transit time estimation using wrist bio-impedance sensing based on a regression model," in *Biomedical Circuits and Systems Conference (BioCAS), 2017 IEEE*, 2017, pp. 1–4.

[13] R. C. Hutchinson, "Mobile Monitoring with Wearable Photoplethysmographic Biosensors," *IEEE Eng. Med. Biol. Mag.*, no. June, 2003.

[14] C. C. Y. Poon, Y. Zhang, T. Chinese, and H. Kong, "A Novel Biometrics Method to Secure Wireless Body Area Sensor Networks for Telemedicine and M-Health," *IEEE Commun. Mag.*, vol. 44.4, no. November 2013, pp. 73–81, 2006.

[15] T. Review, "Photoplethysmography and its application in clinical physiological measurement," *Physiol. Meas.*, vol. 28, no. R1, 2007.

[16] L.-G. Lindberg, H. Ugnell, and P. Å. Öberg, "Monitoring of respiratory and heart rates using a fibre-optic sensor," *Med. Biol. Eng. Comput.*, vol. 30, no. 5, pp. 533–537, 1992.

[17] K. Nakajima, T. Tamura, and H. Miike, "Monitoring of heart and respiratory rates by photoplethysmography using a digital filtering technique," *Med. Eng. Phys.*, vol. 18, no. 5, pp. 365–372, 1996.

[18] H. Kim, J.-Y. Kim, and C.-H. Im, "Fast and robust real-time estimation of respiratory rate from photoplethysmography," *Sensors*, vol. 16, no. 9, p. 1494, 2016.

[19] H.-H. Chang *et al.*, "A method for respiration rate detection in wrist PPG signal using Holo-Hilbert spectrum," *IEEE Sens. J.*, vol. 18, no. 18, pp. 7560–7569, 2018.

[20] J. P. Dieffenderfer *et al.*, "Wearable wireless sensors for chronic respiratory disease monitoring," in *Wearable and Implantable Body Sensor Networks (BSN), 2015 IEEE 12th International Conference on*, 2015, pp. 1–6.

[21] B. Prathyusha, T. S. Rao, and D. Asha, "Extraction of respiratory rate from PPG signals using PCA and EMD," *Int. J. Res. Eng. Technol.*, vol. 1, no. 2, pp. 164–184, 2012.

[22] X. F. Teng and Y.-T. Zhang, "The effect of contacting force on photoplethysmographic signals," *Physiol. Meas.*, vol. 25, no. 5, p. 1323, 2004.

[23] W. S. Johnston and Y. Mendelson, "Extracting breathing rate information from a wearable reflectance pulse oximeter sensor," in *The 26th Annual International Conference of the IEEE Engineering in Medicine and Biology Society*, 2004, vol. 2, pp. 5388–5391.

[24] B. S. Kim and S. K. Yoo, "Motion Artifact Reduction in Photoplethysmography Using Independent Component Analysis," *IEEE Trans. Biomed. Eng.*, vol. 53, no. 3, pp. 2001–2003, 2006.

[25] I. Jeong, D. Bychkov, and P. C. Searson, "Wearable Devices for Precision Medicine and Health State Monitoring," *IEEE Trans. Biomed. Eng.*, vol. 66, no. 5, pp. 1242–1258, 2019.

[26] R. Alonso, A. J. Méndez, and X. A. Vila, "A comparison of three QRS detection algorithms over a public database," *Procedia Technol.*, vol. 9, pp. 1159–1165, 2013.

[27] S. Kontaxis *et al.*, "ECG-derived Respiratory Rate in Atrial Fibrillation," *IEEE Trans. Biomed. Eng.*, 2019.

[28] V. Pichot *et al.*, "ECG-derived respiration : A promising tool for sleep-disordered breathing diagnosis in chronic heart failure patients ☆," *Int. J. Cardiol.*, vol. 186, pp. 7–9, 2015.

[29] G. K. Wolf, J. H. Arnold, and O. Respiratory, "Noninvasive assessment of lung volume: Respiratory inductance plethysmography and electrical impedance tomography," *Crit. Care Med.*, vol. 33, no. 3, pp. 163–169, 2005.

[30] D. Wu *et al.*, "A wearable respiration monitoring system based on digital respiratory inductive plethysmography," *2009 Annu. Int. Conf. IEEE Eng. Med. Biol. Soc.*, pp. 4844–4847, 2009.

[31] T. Elfaramawy *et al.*, "A Wireless Respiratory Monitoring System Using a Wearable Patch Sensor Network," *IEEE Sens. J.*, vol. 19, no. 2, pp. 650–657, 2019.

[32] H. Jin, X. Tao, S. Dong, Y. Qin, L. Yu, and J. Luo, "Flexible surface acoustic wave respiration sensor for monitoring obstructive sleep apnea syndrome," *J. Micromechanics Microengineering*, vol. 27, no. 11, 2017.

[33] D. Lo Presti *et al.*, "Wearable System Based on Flexible FBG for Respiratory and Cardiac Monitoring," *IEEE Sens. J.*, vol. 19, no. 17, pp. 7391–7398, 2019.

[34] S. Chen *et al.*, "Noncontact Heartbeat and Respiration Monitoring Based on a Hollow Microstructured Self-Powered Pressure Sensor," *ACS Appl. Mater. Interfaces*, vol. 10, no. 4, pp. 3660–3667, 2018.

[35] Q. Yang, D. Wang, W. Luo, W. Wang, and M. Lin, "Nano Energy A wearable pyroelectric nanogenerator and self-powered breathing sensor," *Nano Energy*, vol. 38, no. April, pp. 147–154, 2017.

[36] H. Zhang *et al.*, "Waist-wearable wireless respiration sensor based on triboelectric effect," *Nano Energy*, vol. 59, pp. 75–83, 2019.

[37] M. Chattopadhyay and D. Chakraborty, "A New Scheme for Determination of Respiration Rate in Human Being using A New Scheme for Determination of Respiration Rate in Human Being using MEMS Based Capacitive Pressure Sensor : Simulation Study," in *Proceedings of the 8th International Conference on Sensing Technology*, 2014, no. September, pp. 2–7.

[38] P. Sharma, S. S. Member, X. Hui, E. C. Kan, and S. S. Member, "A Wearable RF Sensor for Monitoring Respiratory Patterns * Rx," *2019 41st Annu. Int. Conf. IEEE Eng. Med. Biol. Soc.*, pp. 1217–1223, 2019.

[39] P. S. Kumar *et al.*, "Design and implementation of a bluetooth-based band-aid pulse rate sensor," *Proc. SPIE*, no. April 2011, 2019.

[40] Y. Xiao, C. Li, and J. Lin, "A Portable Noncontact Heartbeat and Respiration Monitoring System Using 5-GHz Radar," *IEEE Sens. J.*, vol. 7, no. 7, pp. 1042–1043, 2007.

[41] X. Li, D. Qiao, Y. Li, and H. Dai, "A novel through-wall respiration detection algorithm using uwb radar," in *Engineering in Medicine and Biology Society (EMBC), 2013 35th Annual International Conference of the IEEE*, 2013, pp. 1013–1016.

[42] T. H. Huynh, R. Jafari, and W.-Y. Chung, "Noninvasive Cuffless Blood Pressure Estimation Using Pulse Transit Time and Impedance Plethysmography," *IEEE Trans. Biomed. Eng.*, vol. 66, no. 4, pp. 967–976, 2019.

[43] B. Ibrahim and R. Jafari, "Cuffless Blood Pressure Monitoring from an Array of Wrist Bio-impedance Sensors using Subject-Specific Regression Models: Proof of Concept," *IEEE Trans. Biomed. Circuits Syst.*, 2019.

[44] W. Lee and S. Cho, "Integrated all electrical pulse wave velocity and respiration sensors using bio-impedance," *IEEE J. Solid-State Circuits*, vol. 50, no. 3, pp. 776–785, 2015.

[45] B. Ibrahim, D. A. Hall, and R. Jafari, "Bio-impedance spectroscopy (BIS) measurement system for wearable devices," in *Biomedical Circuits and Systems Conference (BioCAS), 2017 IEEE*, 2017, pp. 1–4.

[46] J. Xu, P. Harpe, J. Pettine, C. Van Hoof, and R. F. Yazicioglu, "A low power configurable bio-impedance spectroscopy (BIS) ASIC with simultaneous ECG and respiration recording functionality," in *European Solid-State Circuits Conference (ESSCIRC), ESSCIRC 2015-41st*, 2015, pp. 396–399.

[47] C. A. Grant, T. Pham, J. Hough, T. Riedel, C. Stocker, and A. Schibler, "Measurement of ventilation and cardiac related impedance changes with electrical impedance tomography," *Crit. Care*, vol. 15, no. 1, p. R37, 2011.

[48] B. Lobo, C. Hermosa, A. Abella, and F. Gordo, "Electrical impedance tomography," *Ann. Transl. Med.*, vol. 6, no. 2, 2018.

[49] F.-T. Wang, H.-L. Chan, C.-L. Wang, H.-M. Jian, and S.-H. Lin, "Instantaneous respiratory estimation from thoracic impedance by empirical mode decomposition," *Sensors*, vol. 15, no. 7, pp. 16372–16387, 2015.

[50] J.-F. Cardoso, "Blind signal separation: statistical principles," *Proc. IEEE*, vol. 86, no. 10, pp. 2009–2025, 1998.

[51] A. Belouchrani, K. Abed-Meraim, J.-F. Cardoso, and E. Moulines, "A blind source separation technique using second-order statistics," *IEEE Trans. signal Process.*, vol. 45, no. 2, pp. 434–444, 1997.

[52] B. Ibrahim, J. McMurray, and R. Jafari, "A Wrist-Worn Strap with an Array of Electrodes for Robust Physiological Sensing," in *2018 40th Annual International Conference of the IEEE Engineering in Medicine and Biology Society (EMBC)*, 2018, pp. 4313–4317.

[53] K. Sel, D. Kireev, A. Brown, B. Ibrahim, D. Akinwande, and R. Jafari, "Electrical Characterization of Graphene-based e-Tattoos for Bio-Impedance-based Physiological Sensing," in *2019 IEEE Biomedical Circuits and Systems Conference (BioCAS)*, 2019, pp. 1–4.

[54] *Medical electrical equipment Part 1: General requirements for basic safety and essential performance ANSI/AAMI ES60601-1:2005/A1:2012*.

[55] K. Sel, J. Zhao, B. Ibrahim, and R. Jafari, "Measurement of Chest Physiological Signals using Wirelessly Coupled Bio-Impedance Patches," in *2019 41th Annual International Conference of the IEEE Engineering in Medicine and Biology Society (EMBC)*, 2019, p. (accepted).

[56] B. Ibrahim, D. A. Hall, and R. Jafari, "Bio-impedance Simulation Platform using 3D Time-Varying Impedance Grid for Arterial Pulse Wave Modeling," *2019 IEEE Biomed. Circuits Syst. Conf.*, pp. 1–4, Oct. 2019.

[57] A. Morimoto, E. Yasuno, Y. Kinouchi, Y. Ohmine, A. Tangoku, and T. Morimoto, "Spatial resolution in the electrical impedance tomography for the local tissue," in *Annual International Conference of the IEEE Engineering in Medicine and Biology - Proceedings*, 2005, vol. 7 VOLS, pp. 6638–6641.

[58] G. Anand, A. Lowe, and A. M. Al-Jumaily, "Simulation of impedance measurements at human forearm within 1 kHz to 2 MHz," *J. Electr. Bioimpedance*, vol. 7, no. 1, pp. 20–27, 2016.

[59] J. Hurri, A. Hyvärinen, J. Karhunen, and E. Oja, "Image feature extraction using independent component analysis," in *In Proc. NORSIG'96*, 1996.

[60] K. Torkkola, "Blind separation for audio signals-are we there yet?," in *First International Workshop on Independent component analysis and blind source separation*, 1999, pp. 239–244.

[61] S. Amari and A. Cichocki, "Adaptive blind signal processing-neural network approaches," *Proc. IEEE*, vol. 86, no. 10, pp. 2026–2048, 1998.

[62] Y. Zou, V. Nathan, and R. Jafari, "Automatic identification of artifact-related independent components for artifact removal in EEG recordings," *IEEE J. Biomed. Heal. informatics*, vol. 20, no. 1, pp. 73–81, 2016.

[63] T.-P. Jung, S. Makeig, M. Westerfield, J. Townsend, E. Courchesne, and T. J. Sejnowski, "Removal of eye activity artifacts from visual event-related potentials in normal and clinical subjects," *Clin. Neurophysiol.*, vol. 111, no. 10, pp. 1745–1758, 2000.

[64] V. D. Calhoun, T. Adali, J. J. Pekar, and G. D. Pearlson, "Latency (in) sensitive ICA: group independent component analysis of fMRI data in the temporal frequency domain," *Neuroimage*, vol. 20, no. 3, pp. 1661–1669, 2003.

[65] V. D. Vrabie, J. I. Mars, and J.-L. Lacoume, "Modified singular value decomposition by means of independent component analysis," *Signal Processing*, vol. 84, no. 3, pp. 645–652, 2004.

[66] T.-W. Lee, A. Ziehe, R. Orglmeister, and T. Sejnowski, "Combining time-delayed decorrelation and ICA: Towards solving the cocktail party problem," in *Proceedings of the 1998 IEEE International Conference on Acoustics, Speech and Signal Processing, ICASSP'98 (Cat. No. 98CH36181)*, 1998, vol. 2, pp. 1249–1252.

[67] A. C. Tang, M. T. Sutherland, and C. J. McKinney, "Validation of SOBI components from high-density EEG," *Neuroimage*, vol. 25, no. 2, pp. 539–553, 2005.

[68] L. Tong, V. C. Soon, Y.-F. Huang, and R. Liu, "AMUSE: a new blind identification algorithm," in *IEEE international symposium on circuits and systems*, 1990, pp. 1784–1787.

[69] E. Moreau, "A generalization of joint-diagonalization criteria for source separation," *IEEE Trans. Signal Process.*, vol. 49, no. 3, pp. 530–541, 2001.

[70] J. Sakuma, D. Anzai, and J. Wang, "Performance of human body communication-based wearable ECG with capacitive coupling electrodes," *Healthc. Technol. Lett.*, vol. 3, no. 3, pp. 222–225, 2016.

[71] J. F. Zhao, X. M. Chen, B. D. Liang, and Q. X. Chen, "A Review on Human Body Communication: Signal Propagation Model, Communication Performance, and Experimental Issues," *Wirel. Commun. Mob. Comput.*, 2017.

[72] D. Kilani, B. Mohammad, M. Alhawari, H. Saleh, and M. Ismail, "Introduction to Power Management," Springer, Cham, 2020, pp. 1–13.

[73] T. L. Martin and D. P. Siewiorek, "Non-ideal battery properties and low power operation in wearable computing," in *International Symposium on Wearable Computers, Digest of Papers*, 1999, pp. 101–106.

[74] E. Dolan *et al.*, "Superiority of ambulatory over clinic blood pressure measurement in predicting mortality: the Dublin outcome study," *Hypertension*, vol. 46, no. 1, pp. 156–161, 2005.

[75] F. Garcia-Rio *et al.*, "White coat hypertension in patients with obstructive sleep apnea-hypopnea syndrome," *Chest*, vol. 125, no. 3, pp. 817–822, 2004.

Kaan Sel (S'18) is a Ph.D. student in Computer Engineering at Texas A&M University. He received his B.Sc. and M.Sc. degrees in Electrical and Electronics Engineering and B.Sc. (double major) degree in Physics from Middle East Technical University, Ankara, Turkey. His research is focused on designing novel wearable embedded systems and circuits for measurement of vital signs on the human body to be utilized into medical applications and health care.

Bassem Ibrahim (S'12) is a Ph.D. student in Computer Engineering at Texas A&M University. He received his B.Sc. and M.Sc. degrees in Electrical Engineering from Ain Shams University, Cairo, Egypt in 2004 and 2012 respectively. His research interests include the design and development of wearable and reconfigurable health monitoring devices as well as machine learning and signal processing techniques to improve the quality and reliability of the physiological signal. He has 10 years of experience in the design of integrated circuits for sensor chips.

Roozbeh Jafari (SM'12) is a professor of Biomedical Engineering, Computer Science and Engineering and Electrical and Computer Engineering at Texas A&M University. He received his Ph.D. in Computer Science from UCLA and completed a postdoctoral fellowship at UC-Berkeley. His research interest lies in the area of wearable computer design and signal processing. He has raised more than $77M for research with $18M directed towards his lab. His research has been funded by the NSF, NIH, DoD (TATRC), AFRL, AFOSR, DARPA, SRC and industry (Texas Instruments, Tektronix, Samsung & Telecom Italia). He has published over 180 papers in refereed journals and conferences. He has served as the general chair and technical program committee chair for several flagship conferences in the area of Wearable Computers. Dr. Jafari is the recipient of the NSF CAREER award (2012), IEEE Real-Time & Embedded Technology & Applications Symposium best paper award (2011), Andrew P. Sage best transactions paper award (2014), ACM Transactions on Embedded Computing Systems best paper award (2019), and the outstanding engineering contribution award from the College of Engineering at Texas A&M (2019). He has been named Texas A&M Presidential Fellow (2019). He serves on the editorial board for the IEEE Transactions on Biomedical Circuits and Systems, IEEE Sensors Journal, IEEE Internet of Things Journal, IEEE Journal of Biomedical and Health Informatics, IEEE Open Journal of Engineering in Medicine and Biology and ACM Transactions on Computing for Healthcare. He serves on scientific panels for funding agencies frequently, serves as a standing member of the NIH Biomedical Computing and Health Informatics (BCHI) study section (2017-2021), and as the chair of the NIH Clinical Informatics and Digital Health (CIDH) study section (2020).